

Experimental and Modeling Study of Shock-Tube Oxidation of Acetylene

BORIS EITENEER,¹ MICHAEL FRENKLACH²

¹GE Energy and Environmental Research Corporation, 18 Mason, Irvine, California 92618

²Department of Mechanical Engineering, University of California, Berkeley, California 94720-1740

Received 18 December 2002; accepted 23 April 2003

DOI 10.1002/kin.10141

ABSTRACT: Nine mixtures of acetylene and oxygen diluted in argon were studied behind reflected shock waves at temperatures of 1150–2132 K and pressures of 0.9–1.9 atm. Initial compositions were varied from very fuel-lean to moderately fuel-rich, covering equivalence ratios of 0.0625–1.66. Two more mixtures with added ethylene were used to boost the sensitivity to reactions of vinyl oxidation. The progress of reaction was monitored by laser absorption of CO molecules. The collected experimental data were subjected to extensive detailed chemical kinetics analysis. The initial kinetic model was assembled based on recent literature data and then optimized using the solution mapping technique. The analysis was extended to include recent experimental observations of Hidaka and co-workers (*Combust Flame* 1996, 107, 401). The derived model reproduces closely both sets of experimental data, the result obtained by modifying nine rate coefficients and three enthalpies of formation of intermediate species. The identified parameter tradeoffs and justification for the changes are discussed. © 2003 Wiley Periodicals, Inc. *Int J Chem Kinet* 35: 391–414, 2003

INTRODUCTION

High-temperature oxidation of acetylene appears prominent in a variety of natural and industrial processes, such as fossil-fuel combustion [1,2], materials synthesis [3–5], and astrophysical phenomena [6]. The prominence of acetylene stems from its molecular compactness and the nature of the triple carbon–carbon bond, giving rise to the high thermodynamic stability and, at the same time, the high propensity to addition reactions. Reactions of O atoms and OH radicals with accumulating acetylene initiate the secondary chain branching that affects the combustion dynamics of essentially all fuels, including natural gas. Under

fuel-rich conditions, acetylene becomes a major product and plays a critical role in the formation and growth of carbonaceous matter, like polycyclic aromatic hydrocarbons and soot [7–9].

Despite extensive research (see the literature cited in the article), the kinetics of the high-temperature oxidation of acetylene is not yet established with accuracy necessary for predictive numerical modeling. The problems associated with the current kinetic models, those precipitated the present study, are exposed throughout the article. Difficulties encountered in using these kinetics models can be demonstrated, for instance, by a recent numerical analysis of acetylene ignition [10] as well as computer simulations of fuel-rich combustion of natural gas [11].

We report here results of new shock-tube experiments aimed at examining the high-temperature oxidation of acetylene at conditions sensitive to key reactions, and discuss model adopted for the analysis and

Correspondence to: Michael Frenklach; e-mail: myf@me.berkeley.edu.

Contract grant sponsor: Gas Research Institute.
© 2003 Wiley Periodicals, Inc.

document modifications made. We optimize the model, in a systematic and consistent manner, to fit the present shock-tube measurements along with literature experimental data, and conclude with recommendations.

EXPERIMENTAL APPARATUS AND PROCEDURES

The experimental apparatus and procedures were based on those described in our previous studies [12–14]. Briefly, the experiments were performed in a conventional stainless-steel double-diaphragm shock tube with an inner diameter of 8.26 cm, 1.5-m long driver section, and 4.9-m long driven section. The pumping system was upgraded to the Varian 600DS dry scroll mechanical pump, used both as roughing and backing pump, and the Varian Turbo-V 250 turbomolecular pump. This upgraded pumping system is completely oil-free and thus excludes contamination of the vacuum system by the backstreaming pump oil. Prior to each experiment, the test section of the shock tube was evacuated to at least 1×10^{-5} torr. All parts of the gas handling system were tested for leaks with a Varian PortaTest II leak detector. The combined leak-outgassing rate of the driven section was usually about 6×10^{-5} torr min^{-1} . The shock tube was cleaned after each experiment.

The test mixtures were prepared manometrically, with a maximum uncertainty in the final reactant concentrations of less than 1%, and allowed to mix in a stainless-steel tank for at least 24 h prior to experiments. Acetylene of a stated purity higher than 99.6% was obtained from Matheson and was further purified by passing through a series of activated charcoal filters (Matheson Model 454) to ensure removal of acetone impurities [15,16]. The estimated efficiency of our acetone removal technique is 99.9%, much higher than 96% of the dry-ice–acetone cold trap approach [17]. The stated purities for the rest of the gases (all from Matheson) were as follows: argon, 99.9995%; oxygen, 99.997%; helium, 99.999%; ethylene, 99.99%. These gases were used as purchased, without further purification.

The progress of reaction was monitored behind reflected shock waves. The postshock conditions were calculated from the incident shock velocity in the usual manner [18], assuming no chemical reaction and full vibrational relaxation. The thermodynamic data used were based on the standard databases, including the NASA [19] and Technion archives [20,21]. The velocity of the incident shock was extrapolated to the end plate, and this extrapolated value was then used in the calculations of the temperature T_5 , pressure P_5 ,

and total concentration C_5 of gas mixtures behind the reflected shock waves. The observed shock velocity attenuation was less than 2.5% m^{-1} . The uncertainties of reflected shock temperature and pressure were $\pm 0.35\%$ and $\pm 0.09\%$, respectively. Corrections for boundary layer formation were not applied [22].

The concentration of CO was determined by resonance laser absorption [13]. A continuous-wave CO laser was operated at the $2 \rightarrow 1$ P(10) CO transition (2077.1 cm^{-1}). The intensity of the transmitted laser beam was collected at 0.5- μs intervals with the overall time constant of the electro-optical equipment of 0.6 μs . Absolute CO concentrations were determined using the Beer–Lambert law with the collision broadening half-width parameter 4.8×10^{-2} $\text{atm}^{-1} \text{cm}^{-1}$ obtained earlier in our laboratory from CO calibration measurements [13]. Further details can be found elsewhere [17].

EXPERIMENTAL RESULTS

The mixture compositions, experimental conditions, and obtained characteristic times for CO profiles are listed in Table I. Kinetic information was deduced from the experimental data by matching the initial part of the CO profiles, from the onset of reaction up to the maximum in the absorption signal. A sensitivity analysis showed that the remaining part of the CO profiles, after the maximum, was mostly sensitive to reaction $\text{CO} + \text{OH} \rightarrow \text{H} + \text{CO}_2$ and hence did not provide additional information on acetylene reactions. In view of this, each experimental profile was represented by three characteristic points, $t_{1/4}$, $t_{1/2}$, and $t_{3/4}$, the times at which the CO signal reached 1/4, 1/2, and 3/4 of its maximum value, respectively. Taking three points, not one, reflected sensitivity to the reaction chemistry of not just “ignition delay” but also of the shape of the profile.

For numerical analysis each experimental series was represented by five to six sets of optimization targets, $\{\tau_{1/4}, \tau_{1/2}, \tau_{3/4}\}$, chosen as follows. The experimental runs within each series were grouped according to the total concentration C_0 , usually into three groups with C_0 around 7, 9, and 11 mol m^{-3} (see Table I). For each $C_0 \approx \text{const}$ group, experimental characteristic times $t_{1/4}$, $t_{1/2}$, and $t_{3/4}$ were fitted into an Arrhenius-like form and optimization targets τ were selected as representative points of these fits, typically two points near the ends of the temperature range. This procedure allowed us to smoothen experimental variations beforehand and thus to reduce the amount of numerical simulations required. Optimization targets developed following this procedure are listed in Table II.

Table I Experimental Conditions and Results

Experimental Run	T_5 (K)	C_0 (mol m ⁻³)	$t_{1/4}$ (μ s)	$t_{1/2}$ (μ s)	$t_{3/4}$ (μ s)	t_{\max} (μ s)	R_{\max}^a
Series A: 0.25% C ₂ H ₂ -10.00% O ₂ -Ar							
1	1288	10.83	134.4	145.0	154.1	174.0	0.953
2	1303	10.81	136.6	146.4	154.7	171.5	–
3	1336	10.80	128.6	136.9	144.5	163.7	0.826
4	1383	10.78	99.4	105.9	111.4	124.2	0.909
5	1395	10.65	83.5	90.1	95.7	111.1	0.864
6	1463	9.04	85.8	94.8	102.9	119.0	0.876
7	1477	10.77	67.7	73.6	78.6	89.5	0.888
8	1495	8.98	74.2	81.1	86.9	99.5	0.904
9	1519	10.62	51.5	56.7	61.1	71.4	0.902
10	1590	9.21	57.0	63.2	67.8	79.2	0.947
11	1626	9.12	52.2	56.8	61.8	–	0.917
12	1702	9.12	39.2	44.0	47.9	56.6	–
13	1727	7.45	48.4	53.7	57.8	67.6	0.889
14	1731	9.15	34.9	38.6	41.7	50.3	0.874
15	1767	7.58	–	44.7	49.7	59.9	0.921
16	1818	7.54	36.3	40.1	43.8	54.8	0.838
17	1869	7.50	28.3	33.9	38.0	44.7	–
18	1954	7.53	23.6	26.9	30.5	38.7	0.839
19	2081	7.56	19.0	21.8	24.6	32.7	0.810
Series B: 0.50% C ₂ H ₂ -10.10% O ₂ -Ar							
20	1151	12.30	247.2	274.8	295.4	325.6	0.819
21	1161	12.60	208.8	223.9	237.6	259.8	0.906
22	1220	12.51	156.2	167.2	176.8	192.4	0.958
23	1273	12.80	112.4	120.8	127.8	141.1	0.920
24	1352	8.89	104.0	111.7	117.8	129.7	0.865
25	1400	8.88	88.7	95.0	100.1	112.1	0.895
26	1382	12.50	62.1	66.4	70.2	–	–
27	1476	9.08	56.3	60.1	63.5	72.2	0.854
28	1586	9.13	42.8	46.0	49.0	55.9	0.857
29	1697	9.11	29.5	32.2	34.8	41.0	0.849
30	1798	9.28	21.0	23.3	25.8	32.6	0.816
31	1800	7.51	24.3	27.0	28.9	–	–
32	2076	7.93	12.7	14.7	16.6	22.3	0.783
Series C: 0.50% C ₂ H ₂ -5.00% O ₂ -Ar							
33	1182	10.67	346.0	364.7	382.0	–	0.989
34	1247	10.87	249.3	274.6	295.3	330.0	0.957
35	1401	11.32	99.4	106.4	112.2	124.0	0.932
36	1401	11.52	104.7	113.3	120.2	131.6	0.931
37	1416	11.16	81.6	87.7	92.7	104.0	0.914
38	1470	11.15	64.0	68.3	71.9	80.0	0.914
39	1480	8.95	88.1	94.5	99.5	110.3	0.955
40	1589	9.09	60.8	65.4	69.3	79.1	0.908
41	1622	9.05	55.5	59.3	62.8	71.8	0.894
42	1656	9.02	48.2	51.9	55.3	63.0	0.887
43	1702	9.04	41.6	45.0	48.1	55.1	0.894
44	1713	7.33	50.9	55.0	58.5	67.3	–
45	1718	7.34	50.1	54.1	57.8	67.7	0.914
46	1747	9.07	39.0	42.3	45.2	51.5	0.891
47	1820	7.41	38.5	41.8	44.9	52.7	0.891
48	1900	7.46	31.6	34.6	37.4	44.7	0.886

Continued

Table I Continued

Experimental Run	T_5 (K)	C_0 (mol m ⁻³)	$t_{1/4}$ (μ s)	$t_{1/2}$ (μ s)	$t_{3/4}$ (μ s)	t_{\max} (μ s)	R_{\max}^a
Series D: 0.50% C ₂ H ₂ -2.60% O ₂ -Ar							
49	1269	10.85	272.0	312.1	341.8	384.9	0.941
50	1294	10.84	263.5	299.5	335.5	—	0.910
51	1334	8.65	206.3	222.2	235.8	261.8	0.979
52	1349	10.79	157.6	172.9	184.6	209.3	0.929
53	1351	10.81	143.4	162.0	175.7	204.0	0.947
54	1434	10.87	125.7	137.9	147.9	167.5	0.915
55	1441	8.99	142.5	157.8	172.2	197.3	0.900
56	1452	10.80	96.5	105.9	114.0	131.2	0.931
57	1485	9.02	98.2	108.5	117.2	138.2	0.924
58	1491	10.87	99.3	108.9	118.9	133.4	0.939
59	1530	10.80	77.5	85.8	92.9	108.3	0.908
60	1545	10.72	76.9	84.7	90.7	104.7	0.924
61	1566	9.09	82.3	90.0	96.6	112.0	0.915
62	1617	9.09	63.8	69.9	75.2	88.8	0.910
63	1629	8.99	65.9	71.7	76.9	88.5	0.902
64	1646	7.34	77.7	84.5	90.7	104.8	0.928
65	1698	9.02	54.1	59.3	63.7	74.8	0.906
66	1741	9.03	50.6	54.9	59.1	68.6	0.841
67	1747	7.43	56.1	61.7	67.2	79.8	0.888
68	1769	7.37	56.3	61.8	66.6	77.0	0.890
69	1872	7.43	43.1	47.6	51.7	61.0	0.882
70	1912	7.22	31.6	34.9	37.8	44.7	0.885
71	1925	7.38	35.0	38.9	42.5	53.3	0.909
72	2001	7.44	31.6	35.0	38.2	46.9	0.895
73	2004	7.37	29.1	32.4	35.4	43.4	0.885
Series E: 0.50% C ₂ H ₂ -1.25% O ₂ -Ar							
74	1405	10.76	235.9	276.4	308.8	367.4	0.970
75	1406	10.61	199.1	235.9	281.0	—	0.933
76	1412	10.65	171.6	209.4	242.5	300.5	0.938
77	1472	10.69	162.4	188.8	211.5	260.0	0.935
78	1515	9.06	185.9	212.8	235.4	283.6	0.966
79	1520	10.70	134.2	151.6	168.7	201.2	0.952
80	1567	10.75	124.4	142.7	154.7	176.3	0.996
81	1588	10.76	123.6	140.7	155.3	185.8	—
82	1600	9.11	153.3	172.7	198.1	242.0	0.978
83	1630	9.07	124.4	139.7	154.8	187.0	0.946
84	1643	9.07	117.0	130.9	144.1	173.0	0.939
85	1713	7.33	112.3	124.8	138.3	174.0	0.925
86	1729	8.90	90.4	101.8	112.1	135.9	0.926
87	1734	7.34	101.3	114.2	126.5	154.0	0.909
88	1745	9.03	94.0	106.4	120.4	—	—
89	1811	7.39	90.0	99.9	110.9	133.0	0.904
90	1881	7.14	64.2	72.3	79.5	106.0	0.880
91	1887	7.47	73.5	81.5	89.0	109.0	0.922
92	1916	7.38	69.8	77.4	84.7	103.0	0.883
93	1977	7.38	60.5	67.4	74.4	91.5	0.946
Series F: 0.50% C ₂ H ₂ -1.14% O ₂ -Ar							
94	1447	10.72	203.1	236.8	273.6	344.5	0.891
95	1460	10.60	176.8	203.5	238.0	277.4	0.876
96	1483	10.69	182.0	209.1	241.4	308.0	0.897
97	1521	10.62	165.8	190.0	211.5	252.0	0.933
98	1572	6.96	216.8	251.1	283.5	349.0	0.930
99	1578	10.69	142.5	163.3	183.3	221.0	0.920

Continued

Table I Continued

Experimental Run	T_5 (K)	C_0 (mol m ⁻³)	$t_{1/4}$ (μ s)	$t_{1/2}$ (μ s)	$t_{3/4}$ (μ s)	t_{\max} (μ s)	R_{\max}^a
100	1607	9.11	148.1	169.1	188.7	228.4	0.902
101	1656	8.94	113.8	127.1	140.5	171.0	0.909
102	1714	8.98	100.2	112.4	123.7	149.7	0.928
103	1774	8.99	91.2	102.5	113.3	137.0	0.904
104	1813	7.38	96.7	108.1	119.8	148.0	0.923
105	1820	7.43	95.1	105.7	117.2	143.3	0.908
106	1826	7.31	84.7	94.4	103.6	127.4	0.908
107	1950	7.43	65.9	73.5	81.5	100.0	0.946
108	1973	7.39	61.0	68.9	76.5	95.8	0.930
109	2052	7.34	54.0	59.6	65.4	81.5	0.827
Series G: 0.50% C ₂ H ₂ -1.00% O ₂ -Ar							
110	1436	10.69	261.8	–	381.6	477.0	0.993
111	1457	10.62	194.3	234.8	273.8	345.5	0.937
112	1487	10.53	169.5	205.6	249.8	–	0.969
113	1541	10.56	132.5	158.2	184.1	251.5	0.937
114	1591	9.12	179.1	201.6	230.8	284.5	–
115	1632	9.02	145.3	166.5	190.0	235.0	0.938
116	1674	9.01	125.8	146.1	166.1	211.0	0.945
117	1699	8.92	94.6	110.3	124.8	157.0	0.957
118	1737	9.01	102.5	119.7	134.8	163.0	0.927
119	1747	8.94	100.0	113.5	127.5	160.0	0.918
120	1812	6.01	117.3	–	152.4	194.5	0.938
121	1832	7.41	96.2	109.0	122.5	152.0	0.885
122	1882	7.40	83.7	95.3	108.3	135.0	0.934
123	1882	7.30	82.4	93.4	104.1	133.0	0.933
124	1987	7.40	66.9	75.1	83.9	107.5	0.939
125	2006	7.33	57.5	65.0	72.1	90.4	0.929
126	2037	6.27	61.2	69.4	77.4	99.0	0.933
127	2092	6.27	55.9	63.8	72.2	89.5	0.957
128	2132	6.24	44.6	51.1	58.0	75.0	0.889
Series H: 0.50% C ₂ H ₂ -0.89% O ₂ -Ar							
129	1440	10.68	239.9	313.5	387.3	517.7	0.931
130	1465	10.63	226.9	282.1	352.5	473.0	0.953
131	1518	10.66	176.6	213.4	259.4	349.0	0.925
132	1524	9.09	239.9	286.4	337.0	442.4	0.939
133	1537	13.93	142.9	174.0	208.5	289.0	0.946
134	1586	9.12	194.2	232.1	281.8	383.3	0.918
135	1613	9.05	167.7	197.7	229.5	304.5	0.937
136	1621	13.97	105.0	123.5	145.6	206.0	0.969
137	1640	6.52	231.0	266.4	292.4	353.6	0.933
138	1655	9.03	146.9	168.9	192.1	251.0	0.936
139	1719	9.17	125.2	147.0	170.8	218.2	0.908
140	1770	9.17	103.9	119.8	138.8	187.3	0.929
141	1885	6.94	109.7	126.7	144.2	201.5	0.929
142	1885	6.90	92.0	104.6	118.3	154.8	0.912
143	1943	6.89	85.0	96.7	110.4	146.2	0.935
144	1967	6.86	71.0	82.4	93.4	122.2	0.923
145	2032	6.88	64.5	73.6	83.3	110.2	0.939
Series I: 1.00% C ₂ H ₂ -1.51% O ₂ -Ar							
146	1847	6.86	58.3	66.6	75.5	–	–
147	1943	6.91	46.1	52.8	59.7	–	0.842
Series J: 0.346% C ₂ H ₂ -0.087% C ₂ H ₄ -4.323% O ₂ -Ar							
148	1257	11.13	177.0	194.1	209.3	238.0	0.954
149	1271	11.02	204.5	230.9	256.1	295.0	0.905

Continued

Table I Continued

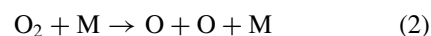
Experimental Run	T_5 (K)	C_0 (mol m ⁻³)	$t_{1/4}$ (μ s)	$t_{1/2}$ (μ s)	$t_{3/4}$ (μ s)	t_{\max} (μ s)	R_{\max}^a
150	1363	11.45	126.8	141.8	155.1	176.0	0.981
160	1394	11.46	105.4	116.1	125.2	142.0	0.944
161	1418	11.14	77.0	84.1	89.9	102.6	0.967
162	1485	11.24	75.1	81.0	86.7	98.0	0.918
163	1519	9.06	73.1	79.7	85.5	97.9	0.915
164	1564	9.07	66.5	72.3	77.3	88.5	0.917
165	1594	9.03	58.0	62.9	67.3	78.8	0.926
166	1649	9.07	49.7	54.0	57.9	67.3	0.893
167	1716	9.11	43.0	47.1	50.7	58.3	0.880
168	1757	9.09	39.5	43.1	46.4	54.9	0.872
169	1794	7.36	45.1	49.2	52.8	63.1	0.880
170	1859	7.42	36.2	40.4	43.9	54.2	0.912
171	1913	7.44	31.9	35.0	38.0	46.2	0.900
172	1989	7.47	26.1	29.0	31.9	40.0	0.903
173	2096	7.57	17.7	20.0	22.3	28.6	0.889
Series K: 0.38% C ₂ H ₂ -0.12% C ₂ H ₄ -1.32% O ₂ -Ar							
174	1444	10.93	173.2	—	273.3	328.0	0.916
175	1454	10.83	174.2	211.8	252.7	310.0	0.944
176	1493	10.80	150.1	173.3	198.0	242.0	1.031
177	1502	10.65	125.5	151.0	173.1	215.0	0.947
178	1539	10.61	112.7	128.1	144.0	176.0	0.915
179	1577	8.97	137.4	160.0	181.4	207.0	0.959
180	1628	9.01	108.1	128.2	147.4	180.0	0.927
181	1667	8.99	100.7	116.3	129.5	159.2	0.959
182	1733	8.98	76.6	87.1	96.0	115.4	0.937
183	1846	7.42	71.2	81.2	90.3	113.1	0.949
184	1851	7.35	71.8	81.3	90.1	105.5	0.995
185	1880	7.27	62.5	70.0	76.9	94.5	0.900
186	1895	7.33	58.0	65.4	72.5	90.0	0.944
187	1996	7.36	42.6	49.0	56.2	71.5	0.962
188	2022	7.34	37.1	42.2	47.1	60.0	0.950

^aObserved ratio of peak CO concentration to total mixture carbon content.

Figure 1 illustrates the CO profile obtained in experimental run 23, Series B at 1273 K (Table I). Also shown in Fig. 1 are model predictions obtained with GRI-Mech 3.0 [23], Hidaka et al.'s mechanism (Model H) [24], Laskin and Wang's mechanism (Model LW) [25], and the trial mechanism assembled in the present study (Model 0). Model H contains 92 reactions of 36 chemical species assembled by Hidaka et al. [24] to simulate their acetylene pyrolysis and oxidation results. Model LW was obtained by adding C₃ and C₄ hydrocarbons' chemistry to GRI-Mech 1.2 and includes 349 reactions of 52 chemical species. Model 0, assembled in the present study, includes 378 reactions of 52 chemical species.

As can be seen in Fig. 1, GRI-Mech 3.0 overpredicts the time of CO appearance by a factor of 5. This is caused mainly by the lack of an initiation step via a reaction between acetylene and molecular oxygen; in GRI-Mech 3.0, the chain process is initiated by the

following reactions:



Also, GRI-Mech 3.0 does not include the chemistry of C₃, C₄, and higher unsaturated hydrocarbons and thus is not suitable for modeling acetylene oxidation, especially at stoichiometric and fuel-rich conditions.

Performance of Models H, LW, and 0 is further illustrated in Fig. 2 for all optimization targets of Table II. The largest discrepancies were observed for targets at low temperatures. Model H predicts experimental characteristic times with an overall accuracy of about +60/−40%. It predicts the peak CO concentrations to be only about 70% of the total carbon content (Fig. 1), while the observed peak CO concentrations accounted for approximately 90% for all experimental conditions

Table II Optimization Targets

Target	T_5 (K)	C_5 (mol m ⁻³)	$\tau_{1/4}$ (μ s)	$\tau_{1/2}$ (μ s)	$\tau_{3/4}$ (μ s)
Series A: 0.25% C ₂ H ₂ -10.00% O ₂ -Ar					
1	1288	10.80	147	156	165
2	1519	10.67	54.8	59.9	64.1
3	1463	9.04	86.4	94.8	102
4	1731	9.16	36.4	40.3	43.8
5	1727	7.50	46.7	51.7	56.3
6	2081	7.56	18.1	21.0	23.9
Series B: 0.50% C ₂ H ₂ -10.10% O ₂ -Ar					
7	1151	12.50	238	260	277
8	1273	12.60	111	119	127
9	1352	8.90	105	112	117
10	1697	9.18	28.7	31.4	34.0
11	1923	7.71	17.8	20.1	22.1
Series C: 0.50% C ₂ H ₂ -5.00% O ₂ -Ar					
12	1182	10.72	367	395	418
13	1470	11.36	67.8	72.9	77.1
14	1480	8.98	88.2	94.4	99.3
15	1747	9.07	38.0	41.1	43.9
16	1718	7.33	50.9	54.9	58.6
17	1900	7.46	31.7	34.7	37.4
Series D: 0.50% C ₂ H ₂ -2.60% O ₂ -Ar					
18	1269	10.87	262	298	327
19	1545	10.80	74.0	80.9	86.9
20	1334	8.80	205	224	241
21	1741	9.11	47.6	52.1	56.1
22	1646	7.37	76.4	83.3	89.7
23	2004	7.37	29.8	33.1	36.2
Series E: 0.50% C ₂ H ₂ -1.25% O ₂ -Ar					
24	1405	10.67	201	239	276
25	1588	10.75	118	134	146
26	1515	8.99	190	215	240
27	1745	9.11	90.1	101	113
28	1713	7.33	110	123	136
29	1977	7.36	59.3	65.9	72.3
Series F: 0.50% C ₂ H ₂ -1.14% O ₂ -Ar					
30	1483	10.66	179	206	236
31	1607	9.05	141	159	177
32	1774	8.96	87.8	98.3	108
33	1572	7.06	212	244	275
34	2052	7.47	51.7	57.2	62.8
Series G: 0.50% C ₂ H ₂ -1.00% O ₂ -Ar					
35	1436	10.65	241	295	351
36	1541	10.53	128	153	180
37	1591	9.11	175	199	228
38	1747	8.96	98.8	114	129
39	1987	7.36	63.3	71.3	79.5
40	1812	6.03	118	134	153
41	2132	6.29	47.6	54.3	61.2
Series H: 0.50% C ₂ H ₂ -0.89% O ₂ -Ar					
42	1572	13.95	125	150	178
43	1465	10.66	220	278	344
44	1524	9.06	239	286	339
45	1770	9.15	105	121	139

Continued

Table II Continued

Target	T_5 (K)	C_5 (mol m ⁻³)	$\tau_{1/4}$ (μ s)	$\tau_{1/2}$ (μ s)	$\tau_{3/4}$ (μ s)
46	1640	6.57	234	270	297
47	2032	6.96	64.2	73.5	83.9
Series I: 1.00% C ₂ H ₂ -1.51% O ₂ -Ar					
48	1894	6.89	51.8	59.3	67.0
Series J: 0.346% C ₂ H ₂ -0.087% C ₂ H ₄ -4.323% O ₂ -Ar					
49	1257	11.14	197	220	241
50	1394	11.35	102	112	121
51	1519	9.05	73.6	79.9	85.4
52	1757	9.10	39.0	42.6	45.8
53	1794	7.36	46.0	50.3	54.0
54	2096	7.56	18.5	20.8	23.2
Series K: 0.38% C ₂ H ₂ -0.12% C ₂ H ₄ -1.32% O ₂ -Ar					
55	1444	10.90	182	227	272
56	1539	10.60	112	127	142
57	1577	8.99	136	160	184
58	1733	8.99	77.4	88.4	97.7
59	1846	7.35	71.6	80.9	89.4
60	2022	7.34	37.8	43.2	48.9

studied. Model LW predicts the peak CO concentrations in good agreement with experiment, and characteristic times with an overall accuracy of about $\pm 30\%$ for equivalence ratios ϕ ranging from 0.50 to 1.66. However, the agreement for the very fuel-lean mixtures is not so close, overpredicting the experimental characteristic times by up to a factor of 4 for mixtures with $\phi = 0.0625, 0.125,$ and 0.25 . The overall agreement with experimental data of the trial mechanism, Model 0, is approximately $+50/-25\%$.

The level of disagreement demonstrated in Figs. 1 and 2 clearly indicates the need for refinement of

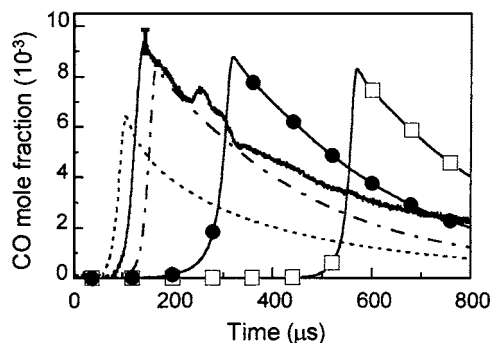


Figure 1 Observed and calculated CO profiles. Experimental conditions are those of experimental run 23 in Table I: 0.50% C₂H₂-10.10% O₂-Ar, $T_0 = 1273$ K, $C_0 = 12.80$ mol m⁻³. Error bars indicate experimental uncertainty in determination of maximum CO concentration. —●—, Experiment; —□—, GRI-Mech 3.0; -----, Model H; —●—, Model LW; - - -, Model 0.

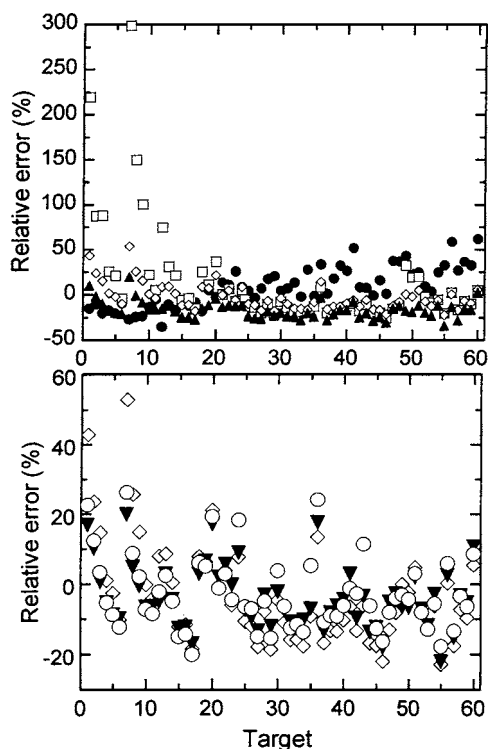


Figure 2 Relative errors defined as $100 \times (\tau_{\text{calc}} - \tau_{\text{expt}}) / \tau_{\text{expt}}$ obtained in numerical predictions of $\tau_{1/2}$. The horizontal axis refers to the experimental targets of Table II. Top panel: ●, Model H; □, Model LW; ◇, Model 0; ▲, Model 0 with the initiation scheme of Hidaka et al. [24]. Bottom panel: ◇, Model 0; ▼, Model 1; ○, Model 2.

high-temperature acetylene oxidation chemistry. This refinement constitutes the subject of the present work.

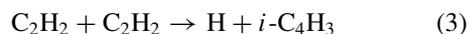
TRIAL MECHANISM

The construction of the trial mechanism, Model 0, for the present study was based on GRI-Mech 3.0 [23]. Additional reactions of C_2H_x , C_3H_x , and C_4H_x species were taken primarily from a recent mechanism of acetylene ignition in shock tubes [25] with further modifications of the kinetic and thermochemical values. These additional reactions and associated rate coefficients [26–47] are listed in Table III. The modifications introduced in the present work are described later.

Initiation Reaction Between C_2H_2 and O_2

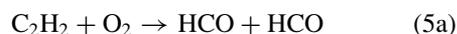
Most of the recent theoretical and experimental studies place the carbon–hydrogen bond energy of acetylene in the range 131–134 kcal mol⁻¹ [48–55]. Such a high

value essentially rules out reactions



as efficient initiation steps under the conditions employed in the present study. Contribution of acetone impurities, suggested by Colket et al. [15,16] to be important during acetylene pyrolysis, can be safely neglected at the expected acetone levels of the present work (see also Kiefer et al. [56]).

Reaction of acetylene with molecular oxygen

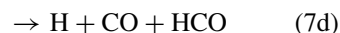


has been proposed as a chain initiation reaction in high-temperature acetylene oxidation [24,28,33,57,58]. Reaction (5d) is generally too slow to compete with channels (5a)–(5c) [33]. Miller et al. [28] and Hidaka et al. [24] reached a conclusion that acetylene ignition delays could not be adequately predicted without reactions (5a)–(5c); however, specific reaction channels cannot be distinguished on the basis of kinetic modeling alone. Hidaka et al. [24] proposed a rate coefficient $k_{5a}^{\text{Hidaka}} = 1.0 \times 10^{12} e^{-14090/T} \text{ cm}^3 \text{ mol}^{-1} \text{ s}^{-1}$ as a fit to their experimental data within the framework of a complex kinetic mechanism, Model H.

Laskin and Wang [25] suggested that reaction between acetylene and molecular oxygen proceeds by isomerization of acetylene to vinylidene [56,59,60],



followed by the reaction between vinylidene and molecular oxygen,



They assumed that the energy barrier for the overall reaction $\text{C}_2\text{H}_2 + \text{O}_2 \rightarrow \text{products}$ is that of the acetylene–vinylidene rearrangement and derived a rate coefficient $k_6^{\text{LW}} = 2.45 \times 10^{15} T^{-0.64} e^{-25010/T} \text{ cm}^3 \text{ mol}^{-1} \text{ s}^{-1}$ for

Table III Reactions Included in Model 0, Additional to GRI-Mech 3.0

No.	Reaction	$k = AT^n \exp(-E/RT)^a$			Comments/Ref.
		A^b ($\text{cm}^3 \text{mol}^{-1} \text{s}^{-1}$)	n	E (cal mol^{-1})	
R1	$\text{C}_2\text{H}_2 + \text{M} \rightleftharpoons \text{H}_2\text{CC} + \text{M}$	2.45(+15)	-0.64	49700	25 ^c
R2	$\text{H}_2\text{CC} + \text{O}_2 \rightleftharpoons \text{CH}_2 + \text{CO}_2$	1.00(+13)			25
R3	$\text{CH}_3 + \text{C}_2\text{H}_2 \rightleftharpoons p\text{-C}_3\text{H}_4 + \text{H}$	2.56(+9)	1.1	13644	36
R4	$\text{CH}_3 + \text{C}_2\text{H}_2 \rightleftharpoons a\text{-C}_3\text{H}_4 + \text{H}$	5.14(+9)	1.1	22153	36
R5	$\text{CH}_3 + \text{C}_2\text{H}_2 \rightleftharpoons \text{CH}_3\text{CCH}_2$	4.99(+2)	-4.4	18850	36
R6	$\text{CH}_3 + \text{C}_2\text{H}_2 \rightleftharpoons a\text{-C}_3\text{H}_5$	2.68(+53)	-12.8	35730	36
R7	$\text{CH}_3 + \text{C}_2\text{H}_3(+\text{M}) \rightleftharpoons \text{C}_3\text{H}_6(+\text{M})$	2.50(+13)			33
		4.27(+58)	-11.94	9770	^d
$a = 0.175, T^{***} = 1341, T^* = 60000, T^{**} = 10140$					^e
R8	$\text{CH}_3 + \text{C}_2\text{H}_3 \rightleftharpoons a\text{-C}_3\text{H}_5 + \text{H}$	1.50(+24)	-2.8	18618	33 ^f
R9	$\text{CH}_3 + \text{HCCO} \rightleftharpoons \text{C}_2\text{H}_4 + \text{CO}$	5.00(+13)			25
R10	$\text{CH}_3 + \text{C}_2\text{H} \rightleftharpoons \text{C}_3\text{H}_3 + \text{H}$	2.41(+13)			33
R11	$\text{C}_2\text{O} + \text{H} \rightleftharpoons \text{CH} + \text{CO}$	5.00(+13)			41
R12	$\text{C}_2\text{O} + \text{O} \rightleftharpoons \text{CO} + \text{CO}$	5.00(+13)			41
R13	$\text{C}_2\text{O} + \text{OH} \rightleftharpoons \text{H} + \text{CO} + \text{CO}$	2.00(+13)			41
R14	$\text{C}_2\text{O} + \text{O}_2 \rightleftharpoons \text{O} + \text{CO} + \text{CO}$	2.00(+13)			41
R15	$\text{HCCO} + \text{OH} \rightleftharpoons \text{C}_2\text{O} + \text{H}_2\text{O}$	3.00(+13)			41
R16	$\text{HCCO} + \text{OH} \rightleftharpoons \text{H} + \text{HCO} + \text{CO}$	1.00(+13)			28
R17	$\text{CH}_2\text{CO} + \text{OH} \rightleftharpoons \text{CH}_2\text{OH} + \text{CO}$	5.00(+12)			46
R18	$\text{CH}_2\text{CO} + \text{CH}_2 \rightleftharpoons \text{C}_2\text{H}_4 + \text{CO}$	1.00(+12)			46
R19	$\text{CH}_2\text{CO} + \text{CH}_2 \rightleftharpoons \text{HCCO} + \text{CH}_3$	3.60(+13)		11000	46
R20	$\text{CH}_2\text{CO} + \text{CH}_3 \rightleftharpoons \text{C}_2\text{H}_5 + \text{CO}$	9.00(+10)			46
R21	$\text{CH}_2\text{CO} + \text{CH}_3 \rightleftharpoons \text{HCCO} + \text{CH}_4$	7.50(+12)		13000	46
R22	$\text{C}_2\text{H}_2 + \text{CH} \rightleftharpoons \text{C}_3\text{H}_2 + \text{H}$	3.00(+13)			30
R23	$\text{C}_2\text{H}_2 + \text{CH}_2 \rightleftharpoons \text{C}_3\text{H}_3 + \text{H}$	1.20(+13)		6620	34
R24	$\text{C}_2\text{H}_2 + \text{CH}_2(\text{s}) \rightleftharpoons \text{C}_3\text{H}_3 + \text{H}$	2.00(+14)			34
R25	$\text{C}_2\text{H}_2 + \text{C}_2\text{H} \rightleftharpoons \text{C}_4\text{H}_2 + \text{H}$	1.77(+13)	0.2	85	See text
R26	$\text{C}_2\text{H}_2 + \text{C}_2\text{H} \rightleftharpoons n\text{-C}_4\text{H}_3$	4.50(+37)	-7.7	7100	42 ^f
R27	$\text{C}_2\text{H}_2 + \text{C}_2\text{H} \rightleftharpoons i\text{-C}_4\text{H}_3$	2.60(+44)	-9.5	14650	42 ^f
R28	$\text{C}_2\text{H}_2 + \text{C}_2\text{H}_2 \rightleftharpoons \text{C}_4\text{H}_4$	1.51(+5)		5500	39
R29	$\text{C}_2\text{H}_2 + \text{C}_2\text{H}_2 \rightleftharpoons \text{C}_4\text{H}_2 + \text{H}_2$	6.31(+13)		42700	39
R30	$\text{C}_2\text{H}_2 + \text{C}_2\text{H}_3 \rightleftharpoons \text{C}_4\text{H}_4 + \text{H}$	2.00(+18)	-1.7	10600	45 ^f
R31	$\text{C}_2\text{H}_2 + \text{HCCO} \rightleftharpoons \text{C}_3\text{H}_3 + \text{CO}$	1.00(+11)		3000	38
R32	$\text{C}_2\text{H}_3 + \text{H}_2\text{O}_2 \rightleftharpoons \text{C}_2\text{H}_4 + \text{HO}_2$	1.21(+10)		-596	33
R33	$\text{C}_2\text{H}_3 + \text{HCO} \rightleftharpoons \text{C}_2\text{H}_4 + \text{CO}$	9.00(+13)			33
R34	$\text{C}_2\text{H}_3 + \text{CH}_3 \rightleftharpoons \text{C}_2\text{H}_2 + \text{CH}_4$	3.92(+11)			33
R35	$\text{CH}_2\text{CHO} + \text{CH}_3 \rightleftharpoons \text{C}_2\text{H}_5 + \text{HCO}$	4.90(+14)	-0.5		28
R36	$\text{CH}_2\text{CHO} \rightleftharpoons \text{CH}_3\text{CO}$	1.00(+13)		47000	26
R37	$\text{CH}_3\text{CO} + \text{M} \rightleftharpoons \text{CH}_3 + \text{CO} + \text{M}$	8.70(+42)	-8.6	22420	33
R38	$\text{CH}_3\text{CO} + \text{H} \rightleftharpoons \text{CH}_3 + \text{HCO}$	9.60(+13)			33
R39	$\text{CH}_3\text{CO} + \text{O} \rightleftharpoons \text{CH}_2\text{CO} + \text{OH}$	3.90(+13)			44
R40	$\text{CH}_3\text{CO} + \text{O} \rightleftharpoons \text{CH}_3 + \text{CO}_2$	1.50(+14)			44
R41	$\text{CH}_3\text{CO} + \text{OH} \rightleftharpoons \text{CH}_2\text{CO} + \text{H}_2\text{O}$	1.20(+13)			33
R42	$\text{CH}_3\text{CO} + \text{OH} \rightleftharpoons \text{CH}_3 + \text{CO} + \text{OH}$	3.00(+13)			33
R43	$\text{CH}_3\text{CO} + \text{HO}_2 \rightleftharpoons \text{CH}_3 + \text{CO}_2 + \text{OH}$	3.00(+13)			33
R44	$\text{CH}_3\text{CO} + \text{H}_2\text{O}_2 \rightleftharpoons \text{CH}_3\text{CHO} + \text{HO}_2$	1.80(+11)		8226	33
R45	$\text{C}_2\text{H}_4 + \text{O} \rightleftharpoons \text{OH} + \text{C}_2\text{H}_3$	1.51(+7)	1.9	3740	41
R46	$\text{C}_2\text{H}_4 + \text{C}_2\text{H} \rightleftharpoons \text{C}_4\text{H}_4 + \text{H}$	1.20(+13)			33
R47	$\text{C}_2\text{H}_4 + \text{O}_2 \rightleftharpoons \text{C}_2\text{H}_3 + \text{HO}_2$	4.22(+13)		60800	33
R48	$\text{C}_2\text{H}_5 + \text{HO}_2 \rightleftharpoons \text{C}_2\text{H}_6 + \text{O}_2$	3.00(+11)			33
R49	$\text{C}_2\text{H}_5 + \text{HO}_2 \rightleftharpoons \text{C}_2\text{H}_4 + \text{H}_2\text{O}_2$	3.00(+11)			33

Continued

Table III Continued

No.	Reaction	$k = AT^n \exp(-E/RT)^a$			Comments/Ref.
		A^b ($\text{cm}^3 \text{mol}^{-1} \text{s}^{-1}$)	n	E (cal mol^{-1})	
R50	$\text{C}_2\text{H}_5 + \text{HO}_2 \rightleftharpoons \text{CH}_3 + \text{CH}_2\text{O} + \text{OH}$	2.40(+13)			33
R51	$\text{C}_2\text{H}_5 + \text{H}_2\text{O}_2 \rightleftharpoons \text{C}_2\text{H}_6 + \text{HO}_2$	8.70(+9)		974	33
R52	$\text{C}_2\text{H}_5 + \text{HCO} \rightleftharpoons \text{C}_2\text{H}_6 + \text{CO}$	1.20(+14)			33
R53	$\text{C}_3\text{H}_2 + \text{O} \rightleftharpoons \text{C}_2\text{H}_2 + \text{CO}$	6.80(+13)			29
R54	$\text{C}_3\text{H}_2 + \text{O} \rightleftharpoons \text{C}_2\text{H} + \text{HCO}$	6.80(+13)			29
R55	$\text{C}_3\text{H}_2 + \text{H} \rightleftharpoons \text{C}_3\text{H}_3$	1.00(+13)			25
R56	$\text{C}_3\text{H}_2 + \text{OH} \rightleftharpoons \text{HCO} + \text{C}_2\text{H}_2$	6.80(+13)			29
R57	$\text{C}_3\text{H}_2 + \text{O}_2 \rightleftharpoons \text{HCCO} + \text{H} + \text{CO}$	2.00(+12)		1000	48
R58	$\text{C}_3\text{H}_2 + \text{CH} \rightleftharpoons \text{C}_4\text{H}_2 + \text{H}$	5.00(+13)			25
R59	$\text{C}_3\text{H}_2 + \text{CH}_2 \rightleftharpoons n\text{-C}_4\text{H}_3 + \text{H}$	5.00(+13)			25
R60	$\text{C}_3\text{H}_2 + \text{CH}_3 \rightleftharpoons \text{C}_4\text{H}_4 + \text{H}$	5.00(+12)			25
R61	$\text{C}_3\text{H}_2 + \text{HCCO} \rightleftharpoons n\text{-C}_4\text{H}_3 + \text{CO}$	1.00(+13)			25
R62	$\text{C}_3\text{H}_3 + \text{H}(+\text{M}) \rightleftharpoons a\text{-C}_3\text{H}_4(+\text{M})$	2.00(+13)			47
		2.29(+56)	-12.55	7934	<i>d</i>
	$a = 0.234, T^{***} = 330, T^* = 4808, T^{**} = 7262$				<i>e</i>
R63	$\text{C}_3\text{H}_3 + \text{H}(+\text{M}) \rightleftharpoons p\text{-C}_3\text{H}_4(+\text{M})$	3.00(+13)			47
		1.60(+57)	-12.59	8376	<i>d</i>
	$a = 0.245, T^{***} = 330, T^* = 3706, T^{**} = 6777$				<i>e</i>
R64	$\text{C}_3\text{H}_3 + \text{H} \rightleftharpoons \text{C}_3\text{H}_2 + \text{H}_2$	5.00(+13)		1000	41
R65	$\text{C}_3\text{H}_3 + \text{O} \rightleftharpoons \text{CH}_2\text{O} + \text{C}_2\text{H}$	2.00(+13)			38
R66	$\text{C}_3\text{H}_3 + \text{OH} \rightleftharpoons \text{C}_3\text{H}_2 + \text{H}_2\text{O}$	2.00(+13)			38
R67	$\text{C}_3\text{H}_3 + \text{OH} \rightleftharpoons \text{C}_2\text{H}_3 + \text{HCO}$	4.00(+13)			47
R68	$\text{C}_3\text{H}_3 + \text{O}_2 \rightleftharpoons \text{CH}_2\text{CO} + \text{HCO}$	3.00(+10)		2868	37
R69	$\text{C}_3\text{H}_3 + \text{HO}_2 \rightleftharpoons \text{OH} + \text{CO} + \text{C}_2\text{H}_3$	8.00(+11)			47
R70	$\text{C}_3\text{H}_3 + \text{HO}_2 \rightleftharpoons a\text{-C}_3\text{H}_4 + \text{O}_2$	1.90(+11)		15000	47
R71	$\text{C}_3\text{H}_3 + \text{HO}_2 \rightleftharpoons p\text{-C}_3\text{H}_4 + \text{O}_2$	3.17(+12)		15000	47
R72	$\text{C}_3\text{H}_3 + \text{HCO} \rightleftharpoons a\text{-C}_3\text{H}_4 + \text{CO}$	2.50(+13)			47
R73	$\text{C}_3\text{H}_3 + \text{HCO} \rightleftharpoons p\text{-C}_3\text{H}_4 + \text{CO}$	2.50(+13)			47
R74	$\text{C}_3\text{H}_3 + \text{CH} \rightleftharpoons i\text{-C}_4\text{H}_3 + \text{H}$	5.00(+13)			47
R75	$\text{C}_3\text{H}_3 + \text{CH}_2 \rightleftharpoons \text{C}_4\text{H}_4 + \text{H}$	5.00(+13)			47
R76	$p\text{-C}_3\text{H}_4 \rightleftharpoons c\text{-C}_3\text{H}_4$	1.20(+44)	-9.9	69250	36 ^f
R77	$p\text{-C}_3\text{H}_4 \rightleftharpoons a\text{-C}_3\text{H}_4$	5.15(+60)	-13.9	91117	36 ^f
R78	$c\text{-C}_3\text{H}_4 \rightleftharpoons a\text{-C}_3\text{H}_4$	4.89(+41)	-9.2	49594	36 ^f
R79	$a\text{-C}_3\text{H}_4 + \text{H} \rightleftharpoons \text{C}_3\text{H}_3 + \text{H}_2$	1.30(+6)	2.0	5500	47
R80	$a\text{-C}_3\text{H}_4 + \text{H} \rightleftharpoons a\text{-C}_3\text{H}_5$	1.52(+59)	-13.5	26949	36 ^f
R81	$a\text{-C}_3\text{H}_4 + \text{O} \rightleftharpoons \text{CH}_2\text{CO} + \text{CH}_2$	2.00(+7)	1.8	1000	47
R82	$a\text{-C}_3\text{H}_4 + \text{OH} \rightleftharpoons \text{C}_3\text{H}_3 + \text{H}_2\text{O}$	5.30(+6)	2.0	2000	25
R83	$a\text{-C}_3\text{H}_4 + \text{CH}_3 \rightleftharpoons \text{C}_3\text{H}_3 + \text{CH}_4$	2.00(+12)		7700	35
R84	$a\text{-C}_3\text{H}_4 + \text{C}_2\text{H} \rightleftharpoons \text{C}_2\text{H}_2 + \text{C}_3\text{H}_3$	1.00(+13)			35
R85	$p\text{-C}_3\text{H}_4 + \text{H} \rightleftharpoons a\text{-C}_3\text{H}_4 + \text{H}$	6.27(+17)	-0.9	10079	36 ^f
R86	$p\text{-C}_3\text{H}_4 + \text{H} \rightleftharpoons \text{CH}_3\text{CCH}_2$	1.66(+47)	-10.6	13690	36 ^f
R87	$p\text{-C}_3\text{H}_4 + \text{H} \rightleftharpoons a\text{-C}_3\text{H}_5$	4.91(+60)	-14.4	31644	36 ^f
R88	$p\text{-C}_3\text{H}_4 + \text{H} \rightleftharpoons \text{C}_3\text{H}_3 + \text{H}_2$	1.30(+6)	2.0	5500	47
R89	$p\text{-C}_3\text{H}_4 + \text{O} \rightleftharpoons \text{HCCO} + \text{CH}_3$	7.30(+12)		2250	47
R90	$p\text{-C}_3\text{H}_4 + \text{O} \rightleftharpoons \text{C}_2\text{H}_4 + \text{CO}$	1.00(+13)		2250	47
R91	$p\text{-C}_3\text{H}_4 + \text{OH} \rightleftharpoons \text{C}_3\text{H}_3 + \text{H}_2\text{O}$	1.00(+6)	2.0	100	47
R92	$p\text{-C}_3\text{H}_4 + \text{CH}_3 \rightleftharpoons \text{C}_3\text{H}_3 + \text{CH}_4$	2.00(+12)	2.0	7700	35
R93	$p\text{-C}_3\text{H}_4 + \text{C}_2\text{H} \rightleftharpoons \text{C}_2\text{H}_2 + \text{C}_3\text{H}_3$	1.00(+13)			47
R94	$a\text{-C}_3\text{H}_5 + \text{H}(+\text{M}) \rightleftharpoons \text{C}_3\text{H}_6(+\text{M})$	2.00(+14)			40
		1.33(+60)	-12.0	5968	<i>d</i>

Continued

Table III Continued

No.	Reaction	$k = AT^n \exp(-E/RT)^a$			Comments/Ref.
		A^b (cm ³ mol ⁻¹ s ⁻¹)	n	E (cal mol ⁻¹)	
$a = 0.200, T^{***} = 1097, T^* = 1097, T^{**} = 6860$					
R95	$a\text{-C}_3\text{H}_5 + \text{H} \rightleftharpoons a\text{-C}_3\text{H}_4 + \text{H}_2$	1.80(+13)			40
R96	$a\text{-C}_3\text{H}_5 + \text{O} \rightleftharpoons \text{C}_2\text{H}_3\text{CHO} + \text{H}$	6.00(+13)			40
R97	$a\text{-C}_3\text{H}_5 + \text{OH} \rightleftharpoons \text{C}_2\text{H}_3\text{CHO} + \text{H} + \text{H}$	4.20(+32)	-5.2	30126	40 ^f
R98	$\text{C}_2\text{H}_3 + \text{HCO} \rightleftharpoons \text{C}_2\text{H}_3\text{CHO}$	1.80(+13)			25
R99	$\text{C}_2\text{H}_3\text{CHO} + \text{H} \rightleftharpoons \text{C}_2\text{H}_4 + \text{HCO}$	1.08(+12)	0.5	1820	25
R100	$\text{C}_2\text{H}_3\text{CHO} + \text{O} \rightleftharpoons \text{C}_2\text{H}_3 + \text{OH} + \text{CO}$	3.00(+13)		3540	25
R101	$\text{C}_2\text{H}_3\text{CHO} + \text{O} \rightleftharpoons \text{CH}_2\text{O} + \text{CH}_2\text{CO}$	1.90(+7)	1.8	220	25
R102	$\text{C}_2\text{H}_3\text{CHO} + \text{OH} \rightleftharpoons \text{C}_2\text{H}_3 + \text{H}_2\text{O} + \text{CO}$	3.43(+9)	1.2	-447	25
R103	$a\text{-C}_3\text{H}_5 + \text{OH} \rightleftharpoons a\text{-C}_3\text{H}_4 + \text{H}_2\text{O}$	6.00(+12)			40
R104	$a\text{-C}_3\text{H}_5 + \text{O}_2 \rightleftharpoons a\text{-C}_3\text{H}_4 + \text{HO}_2$	4.99(+15)	-1.4	22428	43 ^f
R105	$a\text{-C}_3\text{H}_5 + \text{O}_2 \rightleftharpoons \text{CH}_3\text{CO} + \text{CH}_2\text{O}$	1.19(+15)	-1.0	20128	43 ^f
R106	$a\text{-C}_3\text{H}_5 + \text{O}_2 \rightleftharpoons \text{C}_2\text{H}_3\text{CHO} + \text{OH}$	1.82(+13)	-0.4	22859	43 ^f
R107	$a\text{-C}_3\text{H}_5 + \text{HO}_2 \rightleftharpoons \text{C}_3\text{H}_6 + \text{O}_2$	2.66(+12)			44
R108	$a\text{-C}_3\text{H}_5 + \text{HO}_2 \rightleftharpoons \text{OH} + \text{C}_2\text{H}_3 + \text{CH}_2\text{O}$	3.31(+12)			44
R109	$a\text{-C}_3\text{H}_5 + \text{HCO} \rightleftharpoons \text{C}_3\text{H}_6 + \text{CO}$	6.00(+13)			40
R110	$a\text{-C}_3\text{H}_5 + \text{CH}_3 \rightleftharpoons a\text{-C}_3\text{H}_4 + \text{CH}_4$	3.00(+12)	-0.3	-131	40
R111	$a\text{-C}_3\text{H}_5 \rightleftharpoons \text{CH}_3\text{CCH}_2$	7.06(+56)	-14.1	75868	36 ^f
R112	$\text{CH}_3\text{CCH}_2 + \text{H} \rightleftharpoons p\text{-C}_3\text{H}_4 + \text{H}_2$	3.34(+12)			25
R113	$\text{CH}_3\text{CCH}_2 + \text{O} \rightleftharpoons \text{CH}_3 + \text{CH}_2\text{CO}$	6.00(+13)			25
R114	$\text{CH}_3\text{CCH}_2 + \text{OH} \rightleftharpoons \text{CH}_3 + \text{CH}_2\text{CO} + \text{H}$	5.00(+12)			25
R115	$\text{CH}_3\text{CCH}_2 + \text{O}_2 \rightleftharpoons \text{CH}_3 + \text{CO} + \text{CH}_2\text{O}$	4.34(+12)			25
R116	$\text{CH}_3\text{CCH}_2 + \text{HO}_2 \rightleftharpoons \text{CH}_3 + \text{CH}_2\text{CO} + \text{OH}$	2.00(+13)			25
R117	$\text{CH}_3\text{CCH}_2 + \text{HCO} \rightleftharpoons \text{C}_3\text{H}_6 + \text{CO}$	9.00(+13)			25
R118	$\text{CH}_3\text{CCH}_2 + \text{CH}_3 \rightleftharpoons p\text{-C}_3\text{H}_4 + \text{CH}_4$	1.00(+11)			25
R119	$\text{C}_3\text{H}_6 + \text{H} \rightleftharpoons \text{C}_2\text{H}_4 + \text{CH}_3$	8.00(+21)	-2.4	11180	36 ^f
R120	$\text{C}_3\text{H}_6 + \text{H} \rightleftharpoons a\text{-C}_3\text{H}_5 + \text{H}_2$	1.70(+5)	2.5	2490	40
R121	$\text{C}_3\text{H}_6 + \text{H} \rightleftharpoons \text{CH}_3\text{CCH}_2 + \text{H}_2$	4.00(+5)	2.5	9790	40
R122	$\text{C}_3\text{H}_6 + \text{O} \rightleftharpoons \text{CH}_2\text{CO} + \text{CH}_3 + \text{H}$	1.20(+8)	1.6	327	40
R123	$\text{C}_3\text{H}_6 + \text{O} \rightleftharpoons \text{C}_2\text{H}_5 + \text{HCO}$	3.50(+7)	1.6	-972	40
R124	$\text{C}_3\text{H}_6 + \text{O} \rightleftharpoons a\text{-C}_3\text{H}_5 + \text{OH}$	1.80(+11)	0.7	5880	40
R125	$\text{C}_3\text{H}_6 + \text{O} \rightleftharpoons \text{CH}_3\text{CCH}_2 + \text{OH}$	6.00(+10)	0.7	7630	40
R126	$\text{C}_3\text{H}_6 + \text{OH} \rightleftharpoons a\text{-C}_3\text{H}_5 + \text{H}_2\text{O}$	3.10(+6)	2.0	-298	40
R127	$\text{C}_3\text{H}_6 + \text{OH} \rightleftharpoons \text{CH}_3\text{CCH}_2 + \text{H}_2\text{O}$	1.10(+6)	2.0	1450	40
R128	$\text{C}_3\text{H}_6 + \text{HO}_2 \rightleftharpoons a\text{-C}_3\text{H}_5 + \text{H}_2\text{O}_2$	9.60(+3)	2.6	13910	40
R129	$\text{C}_3\text{H}_6 + \text{CH}_3 \rightleftharpoons a\text{-C}_3\text{H}_5 + \text{CH}_4$	2.20(+0)	3.5	5675	40
R130	$\text{C}_3\text{H}_6 + \text{CH}_3 \rightleftharpoons \text{CH}_3\text{CCH}_2 + \text{CH}_4$	8.40(-1)	3.5	11660	40
R131	$\text{C}_4\text{H} + \text{H}(+\text{M}) \rightleftharpoons \text{C}_4\text{H}_2(+\text{M})$	1.00(+17)	-1.0		25
		3.75(+33)	-4.8	1900	^d
$a = 0.646, T^{***} = 132, T^* = 1315, T^{**} = 5566$					
R132	$\text{C}_4\text{H} + \text{O} \rightleftharpoons \text{C}_2\text{H} + \text{C}_2\text{O}$	5.00(+13)			25
R133	$\text{C}_4\text{H} + \text{O}_2 \rightleftharpoons \text{HCCO} + \text{C}_2\text{O}$	5.00(+13)		1500	25
R134	$\text{C}_4\text{H} + \text{H}_2 \rightleftharpoons \text{H} + \text{C}_4\text{H}_2$	4.90(+5)	2.5	560	25
R135	$\text{C}_4\text{H}_2 + \text{H} \rightleftharpoons n\text{-C}_4\text{H}_3$	1.10(+42)	-8.7	15300	25 ^f
R136	$\text{C}_4\text{H}_2 + \text{H} \rightleftharpoons i\text{-C}_4\text{H}_3$	1.10(+30)	-4.9	10800	25 ^f
R137	$\text{C}_4\text{H}_2 + \text{O} \rightleftharpoons \text{C}_3\text{H}_2 + \text{CO}$	2.70(+13)		1720	29
R138	$\text{C}_4\text{H}_2 + \text{OH} \rightleftharpoons \text{H}_2\text{C}_4\text{O} + \text{H}$	6.60(+12)		-410	31
R139	$\text{C}_4\text{H}_2 + \text{OH} \rightleftharpoons \text{C}_4\text{H} + \text{H}_2\text{O}$	3.37(+7)	2.0	14000	25
R140	$\text{H}_2\text{C}_4\text{O} + \text{H} \rightleftharpoons \text{C}_2\text{H}_2 + \text{HCCO}$	5.00(+13)		3000	41
R141	$\text{H}_2\text{C}_4\text{O} + \text{OH} \rightleftharpoons \text{CH}_2\text{CO} + \text{HCCO}$	1.00(+7)	2.0	2000	41
R142	$\text{H}_2\text{C}_4\text{O} + \text{O} \rightleftharpoons \text{CH}_2\text{CO} + \text{C}_2\text{O}$	2.00(+7)	1.9	200	25

Continued

Table III Continued

No.	Reaction	$k = AT^n \exp(-E/RT)^a$			Comments/Ref.
		A^b (cm ³ mol ⁻¹ s ⁻¹)	n	E (cal mol ⁻¹)	
R143	$n\text{-C}_4\text{H}_3 \rightleftharpoons i\text{-C}_4\text{H}_3$	4.10(+43)	-9.5	53000	42 ^f
R144	$n\text{-C}_4\text{H}_3 + \text{H} \rightleftharpoons i\text{-C}_4\text{H}_3 + \text{H}$	2.50(+20)	-1.7	10800	42 ^f
R145	$n\text{-C}_4\text{H}_3 + \text{H} \rightleftharpoons \text{C}_2\text{H}_2 + \text{C}_2\text{H}_2$	6.30(+25)	-3.3	10014	42 ^f
R146	$i\text{-C}_4\text{H}_3 + \text{H} \rightleftharpoons \text{C}_2\text{H}_2 + \text{C}_2\text{H}_2$	2.80(+23)	-2.5	10780	42 ^f
R147	$n\text{-C}_4\text{H}_3 + \text{H} \rightleftharpoons \text{C}_4\text{H}_4$	2.00(+47)	-10.3	13070	42 ^f
R148	$i\text{-C}_4\text{H}_3 + \text{H} \rightleftharpoons \text{C}_4\text{H}_4$	3.40(+43)	-9.0	12120	42 ^f
R149	$n\text{-C}_4\text{H}_3 + \text{H} \rightleftharpoons \text{C}_4\text{H}_2 + \text{H}_2$	3.00(+13)			25
R150	$i\text{-C}_4\text{H}_3 + \text{H} \rightleftharpoons \text{C}_4\text{H}_2 + \text{H}_2$	6.00(+13)			25
R151	$n\text{-C}_4\text{H}_3 + \text{OH} \rightleftharpoons \text{C}_4\text{H}_2 + \text{H}_2\text{O}$	2.00(+12)			25
R152	$i\text{-C}_4\text{H}_3 + \text{OH} \rightleftharpoons \text{C}_4\text{H}_2 + \text{H}_2\text{O}$	4.00(+12)			25
R153	$i\text{-C}_4\text{H}_3 + \text{O}_2 \rightleftharpoons \text{HCCO} + \text{CH}_2\text{CO}$	7.86(+16)	-1.8		25
R154	$\text{C}_4\text{H}_4 + \text{H} \rightleftharpoons n\text{-C}_4\text{H}_3 + \text{H}_2$	6.65(+5)	2.5	12240	25
R155	$\text{C}_4\text{H}_4 + \text{H} \rightleftharpoons i\text{-C}_4\text{H}_3 + \text{H}_2$	3.33(+5)	2.5	9240	25
R156	$\text{C}_4\text{H}_4 + \text{OH} \rightleftharpoons n\text{-C}_4\text{H}_3 + \text{H}_2\text{O}$	3.10(+7)	2.0	3430	25
R157	$\text{C}_4\text{H}_4 + \text{OH} \rightleftharpoons i\text{-C}_4\text{H}_3 + \text{H}_2\text{O}$	1.55(+7)	2.0	430	25
R158	$\text{C}_4\text{H}_4 + \text{CH}_3 \rightleftharpoons n\text{-C}_4\text{H}_3 + \text{CH}_4$	3.98(+11)		4972	32
R159	$\text{C}_4\text{H}_4 + \text{CH}_3 \rightleftharpoons i\text{-C}_4\text{H}_3 + \text{CH}_4$	3.98(+11)		4972	32
R160	$\text{C}_4\text{H}_4 + \text{C}_2\text{H} \rightleftharpoons n\text{-C}_4\text{H}_3 + \text{C}_2\text{H}_2$	3.90(+13)			27
R161	$\text{C}_4\text{H}_4 + \text{C}_2\text{H} \rightleftharpoons i\text{-C}_4\text{H}_3 + \text{C}_2\text{H}_2$	3.90(+13)			27

^a The rate coefficient for the forward direction; the reverse one is calculated via equilibrium constants.

^b Numbers in parentheses denote powers of 10.

^c Third-body enhancement factors: H₂ = 2.0; H₂O = 6.0; CH₄ = 2.0; CO = 1.5; CO₂ = 2.0; C₂H₆ = 3.0; C₂H₂ = 2.5; Ar = 0.7.

^d Low-pressure limit; third-body enhancement factors: H₂ = 2.0; H₂O = 6.0; CH₄ = 2.0; CO = 1.5; CO₂ = 2.0; C₂H₆ = 3.0; Ar = 0.7.

^e Troe's broadening factor $c(T) = (1 - a) \exp(-T/T^{**}) + a \exp(-T/T^*) + \exp(-T^*/T)$.

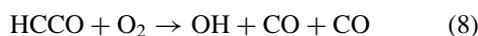
^f Calculated at 760 Torr.

reaction (6) from RRKM calculations based on parameters of Gallo et al. [61]. Channel (7b) was adopted by Laskin and Wang [25] for reaction (7) with a rate coefficient $k_{7b}^{LW} = 1.0 \times 10^{13} \text{ cm}^3 \text{ mol}^{-1} \text{ s}^{-1}$. Using the set of reactions (6) and (7b), Laskin and Wang [25] were able to successfully model shock-tube results of Hidaka et al. [24] on acetylene oxidation.

Our trial mechanism, Model 0, employed the above acetylene–vinylidene initiation scheme of Laskin and Wang [25]. We also tested the direct acetylene–oxygen scheme, using (5a) and k_{5a}^{HHOIA} for the initiation reaction. This worsen the agreement with experiment (Fig. 2), producing a deviation of about 8% in the predicted half-rise times of CO profiles.

Reaction Between HCCO and O₂

Kinetic data on this reaction are very limited. Jones and Bayes [62] carried out an experimental study at 296 K in the discharge flow of helium at 2 torr, and reported a rate constant $1.26 \times 10^{12} \text{ cm}^3 \text{ mol}^{-1} \text{ s}^{-1}$. Miller et al. [28] adjusted it to $1.46 \times 10^{12} e^{-1260/T} \text{ cm}^3 \text{ mol}^{-1} \text{ s}^{-1}$ and assign the reaction products as



Peeters et al. [63] re-investigated reaction (8), at 2 torr helium and temperatures 287 and 535 K, and reported $1.6 \times 10^{12} e^{-430/T} \text{ cm}^3 \text{ mol}^{-1} \text{ s}^{-1}$. The latter recommendation was adopted by Laskin and Wang [25]. The same expression was initially assigned in GRI-Mech and later doubled during the GRI-Mech 3.0 optimization. It should be noted, however, that the sensitivity of the GRI-Mech 3.0 optimization targets to reaction (8) is only marginal [23]. In a recent shock-tube study of ketene oxidation, Hidaka et al. [46] reported that the high-temperature recommendation of Miller et al. [28] gave rise to higher reaction rates than those observed experimentally. Using their kinetic mechanism, Hidaka et al. [46] developed a new expression for the rate coefficient of reaction (8), $4.2 \times 10^{10} e^{-430/T} \text{ cm}^3 \text{ mol}^{-1} \text{ s}^{-1}$. This latter recommendation was adopted for our Model 0.

Reaction C₂H + H₂ → H + C₂H₂

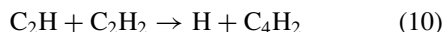
The rate coefficient employed by GRI-Mech 3.0 for reaction



is an extrapolation of Farhat et al.'s recommendation [64], $5.68 \times 10^{10} T^{0.9} e^{-1003/T} \text{ cm}^3 \text{ mol}^{-1} \text{ s}^{-1}$, obtained from their experimental data at 295–854 K. We derived a new expression for this rate coefficient, $4.45 \times 10^6 T^{2.22} e^{-461/T} \text{ cm}^3 \text{ mol}^{-1} \text{ s}^{-1}$, by fitting recent experimental data [64–71] collected over an extended temperature range of 180–4000 K (see Fig. 3).

Reaction $\text{C}_2\text{H} + \text{C}_2\text{H}_2 \rightarrow \text{H} + \text{C}_4\text{H}_2$

The rate coefficient of reaction



used in the present study was a three-parameter fit of recent literature data [64,65,67,68,72,73], $1.94 \times 10^{13} T^{0.238} e^{37/T} \text{ cm}^3 \text{ mol}^{-1} \text{ s}^{-1}$ (see Fig. 4).

C_3H_2

Thermodynamic properties and geometric structures of C_3H_2 isomers are subjects of an ongoing controversy [41,74–90]. On almost all levels of theory an extremely large singlet–triplet split in these compounds causes singlet cyclopropenylidene and singlet vinylidenecarbene to have significantly lower energies than their triplet counterparts, while triplet propargylene has lower energy than its singlet. The scatter in the proposed enthalpies of formation of the most stable C_3H_2 isomers is on the order of several kilocalories [17].

Majority of recent studies has indicated that the most stable form of C_3H_2 is its cyclic isomer, singlet cyclopropenylidene, $c\text{-C}_3\text{H}_2$. An experimental study

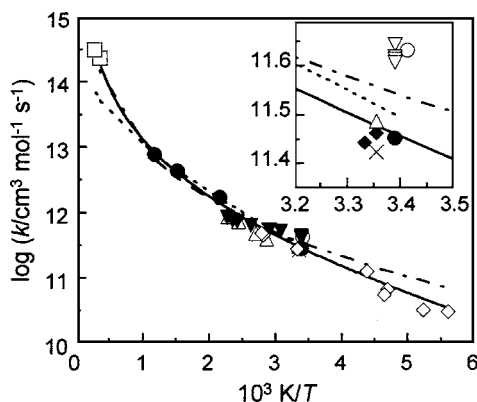


Figure 3 Rate coefficient of reaction $\text{C}_2\text{H} + \text{H}_2 \rightarrow \text{H} + \text{C}_2\text{H}_2$, k_9 . \blacklozenge , Stephens et al. [65]; \times , Lander et al. [66]; \circ , Koshi et al. [67]; \triangle , Koshi et al. [68]; \bullet , Farhat et al. [64]; \blacktriangledown , Peeters et al. [70]; \diamond , Opansky and Leone [69]; \square , Kruse and Roth [71]; \cdots , GRI-Mech 3.0 [23]; $-\cdot-\cdot-$, transition-state-theory calculations of Harding et al. [119] as modified by Peeters et al. [63]; $—$, combined fit, present work.

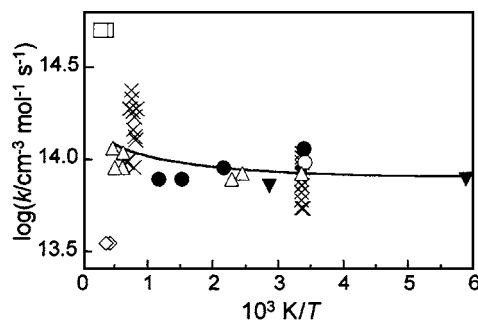
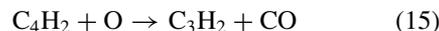
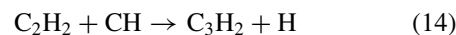
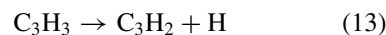
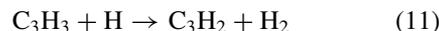


Figure 4 Rate coefficient of reaction $\text{C}_2\text{H} + \text{C}_2\text{H}_2 \rightarrow \text{H} + \text{C}_4\text{H}_2$, k_{10} . \blacklozenge , Stephens et al. [65]; \times , Shin and Michael [72]; \circ , Koshi et al. [67]; \triangle , Koshi et al. [68]; \bullet , Farhat et al. [64]; \blacktriangledown , Pedersen et al. [73]; \diamond , Frank and Just [34]; \square , Kruse and Roth [71]; $—$, combined fit, present work.

of Clauberg et al. [74] led to the enthalpy of formation of $c\text{-C}_3\text{H}_2$ $\Delta_f H_{298}^\circ = 114 \pm 4 \text{ kcal mol}^{-1}$. Chyall and Squires [77] determined an experimental value of $\Delta_f H_{298}^\circ = 119.5 \pm 2.2 \text{ kcal mol}^{-1}$. On the basis of the critical literature review, these authors revised the result of Clauberg et al. [74] to a new value of $120.5 \text{ kcal mol}^{-1}$.

Most of literature sources agree that the second most stable C_3H_2 isomer is triplet propargylene, denoted as C_3H_2 , lying about several kilocalories above singlet $c\text{-C}_3\text{H}_2$. On the basis of an extensive theoretical study and comparison to experimental spectral data, Herges and Mebel [76] concluded that triplet propargylene has a 1,3-diradicaloid C_2 structure rather than C_s carbene structure, $s\text{-C}_3\text{H}_2$. Ochsenfeld et al. [85] calculated almost isoenergetic triplet structures C_s , C_{2v} , and $D_{\infty h}$ lying 0.12, 0.17, and 0.69 kcal mol^{-1} , respectively, above the C_2 structure. Seburg et al. [86,91] performed ^{13}C labeling of C_3H_2 photochemical precursors and also concluded that triplet propargylene has C_2 allene diradical-like geometry rather than the C_s acetylene carbene-like structure.

The formation of C_3H_2 is described in Model 0 mostly through the following reactions:



Miller and co-workers [79] suggested that triplet propargylene is the most likely product of reaction (11), the dominant formation path of C_3H_2 in their $\text{H}_2/\text{O}_2/\text{Ar}-\text{C}_3\text{H}_4$ flame. Although these authors did not

exclude the possibility of formation of other C_3H_2 isomers in their flames, they modeled the C_3H_2 species as triplet propargylene in their kinetic scheme [79,81]. Kiefer et al. [84] considered reactions (11) and (13) as the source of C_3H_2 in their shock-tube experiments. These authors showed that even assuming that cyclopropenylidene is the most stable isomer energetically, the triplet propargylene is by far the dominant isomer at equilibrium in the temperature range 1500–2500 K (see their Fig. 12), with a relative amount of cyclopropenylidene increasing toward lower temperatures. Boullart et al. [92] described reaction (14) as the source of C_3H_2 in their $C_2H_2/O/H$ flames. These authors compared the approximate ionization potential 9.5 ± 0.4 eV observed for C_3H_2 with the experimental value of 9.15 ± 0.03 eV for $c-C_3H_2$ [74] and a theoretical value of 8.7 eV for triplet propargylene, C_3H_2 [74]. Based on this comparison, Boullart et al. [92] concluded that in their system at 600 K the C_3H_2 is largely singlet cyclopropenylidene. This conclusion is in qualitative agreement with equilibrium calculations of Kiefer et al. [84]. Guadagnini et al. [87] argued that reaction (11) with an exit barrier for the $c-C_3H_2$ channel should favor formation of linear C_3H_2 . Detailed microcanonical RRKM master equation calculations performed by Vereecken and Peeters [90] on product distribution of reaction (11) showed that the yield of the triplet HCCCH isomer changed from 90% at 300 K to 82% at 2000 K for pressures from 0 to 5 atm. In contrast, Deyerl et al. [93] proposed based on their experimental data and RRKM analysis that photodissociation of the propargyl radical results predominantly in the formation of cyclopropenylidene.

The above information indicates uncertainties associated with the thermodynamic and kinetic data of C_3H_2 isomers. The experimental and theoretical

evidence suggests that the major isomer of C_3H_2 formed under the conditions of the present experimental study should be the triplet propargylene having the 1,3-diradicaloid C_2 structure. Because of the large scatter and scarcity of the thermodynamic data for this species, several high-level ab initio calculations, at B3LYP/cc-pVTZ, G2, and G3 levels of theory, were performed in our laboratory [94] to assess the geometric structure and energetics of triplet propargylene. The G3 results [17], with $\Delta_f H_{298}^\circ = 130.4$ kcal mol⁻¹, were adopted for Model 0, and subjected to optimization against Hidaka et al.'s experimental data.

C_4H_3

Model 0 includes reactions of two C_4H_3 isomers, $n-C_4H_3$ and $i-C_4H_3$ (Table III). A review of literature [16,20,21,24,25,41,47,56,95–97] reveals significant scatter in the standard enthalpies of formation for these species. Recently, a series of quantum ab initio, density-functional, and Quantum Monte Carlo calculations were performed for the enthalpy of formation of $n-C_4H_3$ and $i-C_4H_3$ radicals [98]. The initial G3 results, as documented in [17], were adopted for Model 0, and subjected to optimization against Hidaka et al.'s experimental data.

MODEL OPTIMIZATION

Optimization Variables

Model 0, assembled as discussed earlier, served as the first trial mechanism for modeling the present shock-tube experiments on acetylene oxidation. A screening sensitivity analysis performed for the experimental targets of Table II are displayed in Fig. 5. The highest

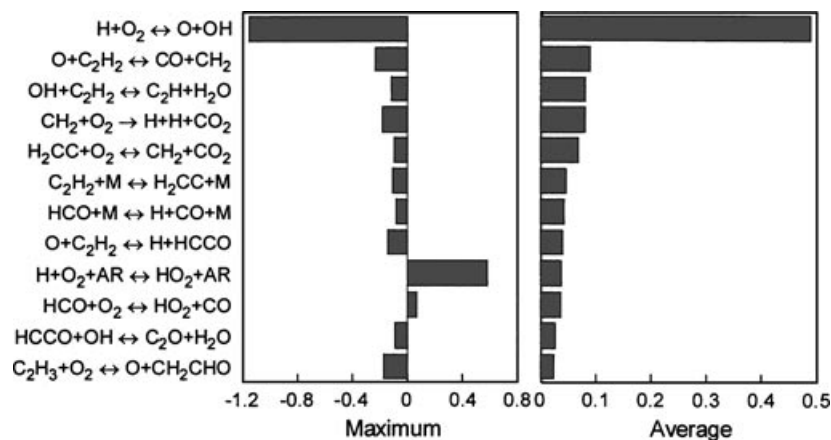
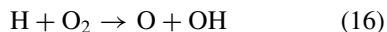
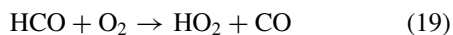


Figure 5 Logarithmic response sensitivities computed for the half-rise time $t_{1/2}$ of CO signal with Model 0. The average values are arithmetic means of absolute sensitivities for all targets included in Table II. Only values above 0.05 are shown.

sensitivities correspond to reactions



Their rate coefficients are known with high accuracy [23,99,100] and hence were fixed at the corresponding GRI-Mech 3.0 expressions and not included into parameter optimization. Reactions

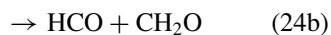
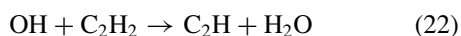
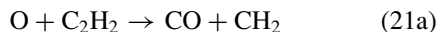


were studied in our previous work [14] as part of the formaldehyde submechanism. Their rate coefficients were fixed at the GRI-Mech 3.0 values and excluded from the present parameter optimization. Reaction



displayed only marginal sensitivity and hence was not included into the optimization.

Optimization against the experimental targets of Table II included reactions (6), (7b), and



Reaction (24b) does not appear in Fig. 5 due to its low sensitivity, but was included into the optimization process to achieve a better control over the total rate and the branching ratio of reaction (24). The starting values for k_6 and k_{7b} were those of Laskin and Wang [25], expressions k_6^{LW} and k_{7b}^{LW} , respectively. The starting expressions for the rate coefficients of reactions (21a), (21b), (22), (23), (24a), and (24b) were those of GRI-Mech 3.0 [23]. Initially, the pre-exponential factors and activation energies of all listed rate coefficients were set as free optimization variables. However, it was noticed in the initial phase of optimization that allowing changes in activation energies of reactions (22), (23), (24a), and (24b) did not produce much improvement in fitting the experimental targets. Consequently, activation energies of these reactions were fixed at the corresponding GRI-Mech 3.0 values.

Optimization Runs

The results of a series of optimization runs are summarized in Table IV. The objective function for optimization was defined as

$$\Phi = \sum_{\text{all responses}} \sum_{\substack{i=1/4, \\ 1/2, \\ 3/4}} \left(\frac{\tau_{i,\text{calc}} - \tau_{i,\text{exp}}}{\tau_{i,\text{exp}}} \right)^2.$$

The first two rows of Table IV document the least-square residuals computed with Models H and LW. The next row, Case I, lists the results obtained with Model 0. Comparison of the respective Φ values shows that, overall, Model H performs close to Model 0, and the two have much lower Φ than Model LW. As discussed earlier, predictions of Model LW are close to those of Model 0 for our mixtures D through K, but Model 0 shows a significant improvement over Model LW for the most fuel-lean mixtures, A, B, and C (Table I). The improvement comes solely from the replacement of the GRI-Mech 1.2 module of Model LW with the updated version, GRI-Mech 3.0. The differences in the thermodynamic properties of the C_3H_2 and C_4H_3 species between Model 0 and Model LW result only in minor changes of model predictions for the current experimental targets. However, their influence grows with the increase in mixture concentration and equivalence ratio, as will be witnessed in modeling of Hidaka et al.'s experiments [24] described in a later section.

Case II was a free optimization run with all pre-exponential factors set free. Its result, $\Phi_{\text{II}} = 1.53$, represents an effective lower limit of the objective function. The free optimization shows a moderate reduction in the objective function from the reference case of Model 0, $\Phi_{\text{I}} = 4.27$. Yet, as is often the case, several parameters reached the optimization boundaries during free optimization: k_{23} reached the upper boundary, while k_6 , k_{7b} , k_{21b} , and k_{24b} reached lower boundaries of the respective optimization ranges. Hence, constrained optimization followed. Case III repeated the free optimization of Case II but with k_{24a} and k_{24b} fixed at the GRI-Mech 3.0 expressions. Comparison of Cases II and III showed that the influence of rate coefficients k_{24a} and k_{24b} is marginal, consistent with the sensitivity analysis (Fig. 5). Cases IV–VI further demonstrate this conclusion. Therefore, the rate coefficients of reactions (24a) and (24b) were fixed at the corresponding GRI-Mech 3.0 expressions and not included into further optimization runs.

Cases VII and VIII explored the influence of pre-exponential factors A_6 and A_{7b} , respectively, whereas Case IX allowed for simultaneous changes in A_6 and A_{7b} . Addition of activation energies of reactions (6) and

Table IV Results of Model Optimization Against Targets Listed in Table II

Case	Optimization Variables ^a												Objective Function Φ
	A_6	E_6	A_{7b}	E_{7b}	A_{21a}	E_{21a}	A_{21b}	E_{21b}	A_{22}	A_{23}	A_{24a}	A_{24b}	
Model H													9.25
Model LW													61.49
I	1		1		1		1		1	1	1	1	4.27
II	0.33 ₋		0.33 ₋		2.13		0.50 ₋		0.39	2.00 ⁺	0.42	0.40 ₋	1.45
III	0.33 ₋		0.33 ₋		2.09		0.50 ₋		0.37	2.00 ⁺	1	1	1.53
IV	1		1		1		1		1	1	1	0.40 ₋	3.96
V	1		1		1		1		1	1	1.45	1	4.21
VI	1		1		1		1		1	1	0.96	0.40 ₋	3.95
VII	2.11		1		1		1		1	1	1	1	4.02
VIII	1		0.68		1		1		1	1	1	1	4.10
IX	3.00 ⁺		0.49		1		1		1	1	1	1	3.14
X	2.00 ⁺	-2000 ₋	0.50 ₋	-188	1		1		1	1	1	1	2.87
XI	1		1		1		1		1	1.39	1	1	4.00
XII	1		1		1		1		0.83	1	1	1	4.23
XIII	1		1		1		0.67		1	1	1	1	4.19
XIV	1		1		1.47		1		1	1	1	1	3.80
XV	1		1		1.52		0.50 ₋		1	1	1	1	3.26
XVI	1		1		1.86		0.50 ₋		0.33 ₋	1.16	1	1	2.08
XVII	1		1		2.10		0.50 ₋		0.33 ₋	1	1	1	2.09
XVIII	3.00 ⁺		0.33 ₋		1.85		0.50 ₋		1	1	1	1	1.89
XIX	1		0.33 ₋		2.11		0.50 ₋		1	1	1	1	1.99
XX	1		0.33 ₋		2.69		0.50 ₋		0.49	1	1	1	1.68
XXI	0.49		0.33 ₋		3.00 ⁺		0.50 ₋		0.51	1	1	1	1.68
XXII	1		0.33 ₋		2.17		<u>0.75</u>		1	1	1	1	2.19
XXIII	1		0.33 ₋		2.22		1		1	1	1	1	2.38
XXIV	1		0.50 ₋		1.85		0.50 ₋		1	1	1	1	2.36
XXV	1		0.33 ₋		1.58	-1000 ₋	<u>0.75</u>	-1000	1	1	1	1	2.24
XXVI	0.33 ₋		0.33 ₋		1.46	-1000 ₋	0.50 ₋		0.40 ₋	2.00 ⁺	1	1	1.46
XXVII	1		0.33 ₋	2000 ⁺	2.68		0.50 ₋		1	1	1	1	1.73
XXVIII	1		0.33 ₋		1.57		0.50 ₋		<u>2.00</u>	1	1	1	2.89
XXIX	3.00 ⁺		0.33 ₋		1.37		0.50 ₋		<u>2.00</u>	1	1	1	2.68
XXX	3.00 ⁺		0.33 ₋		1.40		0.50 ₋		<u>2.00</u>	0.97	1	1	2.68
XXXI	1		0.33 ₋		1.63		0.50 ₋		<u>2.00</u>	0.95	1	1	2.88
XXXII	1		0.33 ₋		1.55		<u>0.75</u>		<u>2.00</u>	1	1	1	3.10
XXXIII	1		0.33 ₋		1.79		0.50 ₋		<u>1.50</u>	1	1	1	2.44
XXXIV	2.00 ⁺		0.33 ₋		1.63		0.50 ₋		<u>1.50</u>	1	1	1	2.36
XXXV	2.00 ⁺		0.33 ₋		1.61		<u>0.70</u>		<u>1.50</u>	1	1	1	2.52
XXXVI	1		0.33 ₋		1.80		<u>0.70</u>		<u>1.50</u>	1	1	1	2.60
XXXVII	2.00 ⁺		0.33 ₋		1.62		<u>0.65</u>		<u>1.50</u>	1	1	1	2.48
XXXVIII	1		0.33 ₋		1.80		<u>0.60</u>		<u>1.50</u>	1	1	1	2.52
XXXIX	1		1		1		1		<u>1.50</u>	1	1	1	4.66

^a Entry designations are as follows: 1 for a pre-exponential factor and an empty entry for an activation energy indicates that the corresponding value was fixed at the Model 0 expression. Numerical entry followed by + (in superscript) or - (in subscript) sign indicates that the optimization variable reached the upper or lower boundary of the optimization range, respectively. Underlined numerical entry indicates that the value was fixed during the optimization.

(7b) as optimization variables, Case X, did not produce a significant improvement in the objective function, yet forced the rate coefficient k_6 above the chosen upper limit 3.00 of the optimization range. Cases XI–XVII tested the interplay among the rate coefficients of reactions (21a), (21b), (22), and (23). A major improve-

ment in the objective function came from simultaneous optimization of rate coefficients k_{21a} , k_{21b} , and k_{22} (Case XVII). When set free (Cases XVI and XI), the optimized values of k_{23} were close to 1; hence the rate coefficient k_{23} was fixed at the starting expression and optimized no further.

Cases XVIII–XXI examined the interaction among the rate coefficients of reactions (6), (7b), (21a), (21b), and (22). Case XIX showed that inclusion of k_{7b} into optimization instead of k_{22} resulted in approximately the same quality of fit to experimental data as Case XVII. Simultaneous optimization of k_{21a} , k_{21b} , k_{22} , and k_{23} , Case XX, did not significantly reduce the objective function compared to Cases XVII and XIX, but resulted in further departure of k_{23} from the starting expression. As the rate coefficient k_{22} is better established than simply estimated k_{7b} (see, e.g., Baulch et al. [101] and references therein), optimization Case XIX is preferred in the current study to Case XVII.

Cases XIX and XXII–XXVII illustrate a trade-off between changing the branching ratio and the total rate of reaction (21). Case XIX showed that $\Phi_{XIX} = 1.99$, close to the minimum value of $\Phi_{III} = 1.53$, could be reached just by changing the branching ratio of reaction (21), $BR_{21} = k_{21b}/(k_{21a} + k_{21b})$, and the pre-exponential factor of reaction (7b). Compared to the starting GRI-Mech 3.0 expressions, Case XIX reversed the branching ratio of channels (21a) and (21b) while leaving the total rate of reaction (21) essentially unchanged. Case XXIII resulted in almost equal rates of channels (21a) and (21b), or $BR_{21} = 0.5$, and an increase in the total rate of reaction (21) by about 40%. Case XXII led to the BR_{21} value intermediate between Cases XIX and XXIII. Case XXV gave rise to $BR_{21} = 0.5$ while decreasing the activation energy of reaction (21), E_{21} , by 1 kcal mol⁻¹. Such a change in E_{21} would lead to significantly overestimated rate of reaction (21) at low temperatures.

Additional optimization runs, Cases XXVIII–XXXIX, were performed to assess the influence of increased k_{22} on the optimized values of k_6 , k_{7b} , k_{21a} , k_{21b} , and k_{23} ; its significance will be discussed in the next section.

Summary of Optimization Results

Considering the trends revealed by the results of optimization and taking into account the uncertainties in literature recommendations, we select Case XIX as a tentative choice.

Optimization performed over the present acetylene oxidation targets indicates that a major improvement in agreement between the model and experiment comes from optimized rate coefficients of reaction $O + C_2H_2$, channels (21a) and (21b), and reaction (7b). A three-fold decrease in the rate coefficient of reaction (7b) is suggested by many optimization runs, and it can be accepted considering the estimated character of k_{7b} (see Laskin and Wang [25]). Reduction of k_{7b} by a factor

of 3 from the base expression leads to $k_{7b}^{XIX} = 3.3 \times 10^{12} \text{ cm}^3 \text{ mol}^{-1} \text{ s}^{-1}$.

As mentioned earlier, recommendations [23,34, 102–118] for the total rate coefficient of reaction (21) are in a reasonable agreement with each other (Fig. 6), yet there is a significant scatter in the branching ratio of this reaction [17,101,119]. The branching ratio employed by Model 0 is taken from GRI-Mech 3.0, $BR_{21}^{GRI-Mech3.0} = 0.66$. Optimization Case XIX resulted in $BR_{21}^{XIX} = 0.33$ while leaving the total rate of reaction (21) essentially unchanged. We will return to this issue at our final recommendations.

We will refer to the reaction mechanism with the Case XIX parameter set as Model 1. A comparison in performance of Models 0 and 1 against the experimental data of Table II is shown in the bottom panel of Fig. 2. As can be seen, Model 1 exhibits substantial improvements over Model 0, with relative errors in the predicted half-rise times of CO profiles within $\pm 20\%$ for all experimental conditions studied.

MODEL VALIDATION AND FURTHER OPTIMIZATION

Prior to making final conclusions, we tested the tentative result of our optimization, Model 1, against another set of experimental data, recently reported shock-tube

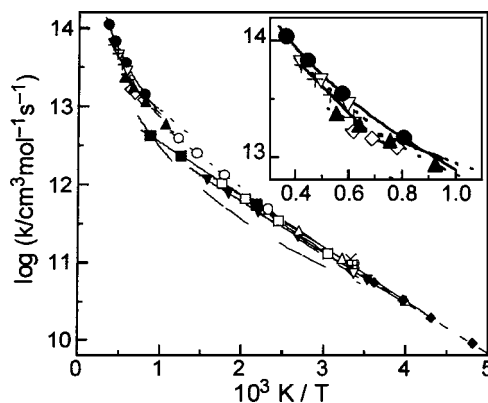


Figure 6 Literature recommendations for the rate coefficient of reaction $O + C_2H_2 \rightarrow \text{products}$, $k_{21} = k_{21a} + k_{21b}$. \square , Sullivan and Warneck [102]; \times , Niki [103]; \square , Brown and Thrush [104]; $-\cdot-\cdot-$, James and Glass [105]; $-\blacktriangledown-$, Hoyermann et al. [106]; $-\triangle-$, Westenberg and de Haas [107]; \blacklozenge , Stuhl and Niki [108]; $-\diamond-$, Peeters and Mahnen [109]; $-\cdot-\cdot-$, Vandooren and Van Tigglen [110]; ∇ , Westenberg and de Haas [111]; $-\square-$, Aleksandrov et al. [112]; $---\nabla---$, Lohr and Haas [113]; $-\blacksquare-$, Homann and Wellman [114]; $-\cdot-\cdot-$, Frank et al. [34]; $-\cdot-\cdot-$, Mahmud and Fontijn [115]; $-\cdot-\cdot-$, Russell et al. [116]; $-\blacklozenge-$, Bohn and Stuhl [117]; $-\blacktriangle-$, Michael and Wagner [118]; $-\bullet-$, GRI-Mech 3.0 [23].

oxidation of acetylene by Hidaka et al. [24]. It turned out that essentially all the models we considered—GRI-Mech 3.0, LW, Model 0, and Model 1—had difficulty in explaining those observations, as illustrated in Fig. 7. On the other hand, Model H developed by the authors [24] by fitting their results does not predict closely the experimental data of the present work, as can be seen in the top panel of Fig. 2. To resolve this apparent disagreement, we subjected the Hidaka et al.'s data to the same type of analysis we applied to our own data, i.e., we subjected those data to optimization starting with our Model 1.

Target Development

The derived experimental targets are listed in Table V. Targets HID-6A and HID-6B were obtained from the concentration profiles of O₂ and C₂H₂ (Figs. 6a and 6b in [24]); $\tau_{1/2}$ and $\tau_{3/4}$ represent the times when O₂ or C₂H₂ concentration reached 1/2 and 3/4 of the initial value, respectively. Target HID-6C was developed based on CO concentration profile (Fig. 6c in [24]); $\tau_{1/4}$ and $\tau_{1/2}$ represent the times when CO concentration reached 1/4 and 1/2, respectively, of its maximum value. The maximum CO concentration, not shown in Fig. 6c of Hidaka et al. [24], was calculated using Model H.

Targets HID-7A, HID-7B, and HID-7C were obtained from the reported emission profiles at 4.24 μm (Figs. 7a–7c in [24]). Hidaka and co-workers [24] concluded that the main source of IR emission observed at 4.24 μm in their experiments was CO₂. We calculated the CO₂ emission intensity using their reported expression [46] $I_e = 10^{T/2985+7.20} [\text{CO}_2]$, where T in K, $[\text{CO}_2]$ in $\text{cm}^3 \text{mol}^{-1}$, and I_e in mV. Calculations using Model H showed that the experimental emission profiles could be approximated by CO₂ concentration

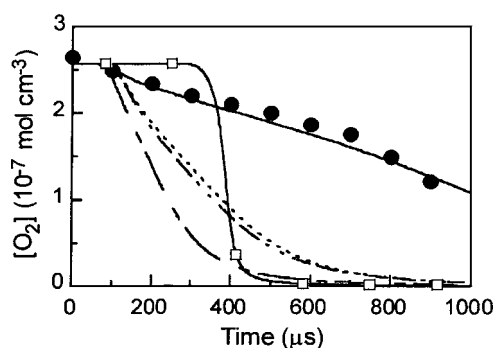


Figure 7 Observed and calculated O₂ profiles. Experimental conditions: 4.0% C₂H₂–2.0% O₂–Ar; $T_0 = 1273 \text{ K}$; $C_0 = 12.9 \text{ mol m}^{-3}$. ●, experiment (Hidaka et al. [24]); –□–, GRI-Mech 3.0; – – –, Model LW; ·····, Model 0; – · – ·, Model 1; —, Model 2.

Table V Optimization Targets for Acetylene Oxidation Based on Experimental Observations of Hidaka et al. [24]

Target	T_5 (K)	C_5 (mol m^{-3})	$\tau_{1/4}$ (μs)	$\tau_{1/2}$ (μs)	$\tau_{3/4}$ (μs)
Series 1: 4.0% C ₂ H ₂ –2.0% O ₂ –Ar					
HID-6A ^a	1273	12.9	–	871	543
HID-6B ^b	1343	13.4	–	725	344
HID-6C ^c	1292	13.0	527	826	–
Series 2: 1.0% C ₂ H ₂ –2.5% O ₂ –Ar					
HID-7A ^d	1221	14.5	339	421	655
Series 3: 1.0% C ₂ H ₂ –5.0% O ₂ –Ar					
HID-7B ^d	1214	14.5	150	190	322
Series 4: 2.0% C ₂ H ₂ –2.5% O ₂ –Ar					
HID-7C ^d	1179	14.3	566	715	826

^a O₂ decay, mass spectrometry.

^b C₂H₂ decay, mass spectrometry.

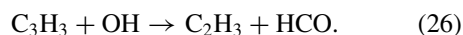
^c CO rise, mass spectrometry.

^d CO₂ rise, IR emission.

profiles with an accuracy of about 5% for targets HID-7A and HID-7C. For target HID-7B, however, the differences between the emission and the CO₂ concentration profiles were significantly higher, about 15%. On the basis of this observation, the target HID-7B of Table V was excluded from the present optimization, although the comparisons with the experimental emission data were performed (see later). For targets HID-7A and HID-7B, the values of $\tau_{1/4}$, $\tau_{1/2}$ and $\tau_{3/4}$ listed in Table V are the times when emission calculated using the above expression for I_e and Model H reached 1/4, 1/2, and 3/4 of its value at 2000 μs , and for target HID-7C of its maximum value. The compound errors in determination of the target values, because of approximations involved, are estimated to be about 5–10%.

Optimization Variables

Figure 8 displays a sensitivity spectrum calculated for the experimental conditions of Fig. 7 with Model 0. Reaction (16) has the largest sensitivity for all targets of Table V, as expected. Its rate coefficient, k_{16} , was fixed at the GRI-Mech 3.0 expression, as previously, and not included into optimization. The optimization variables were chosen according to the rest of the sensitivity ranking and included the pre-exponential factors of reactions (22), (24a), (24b), and



The sensitivity of the Hidaka et al.'s targets to k_{7b} , k_{21a} , and k_{21b} is very small (which explains the small

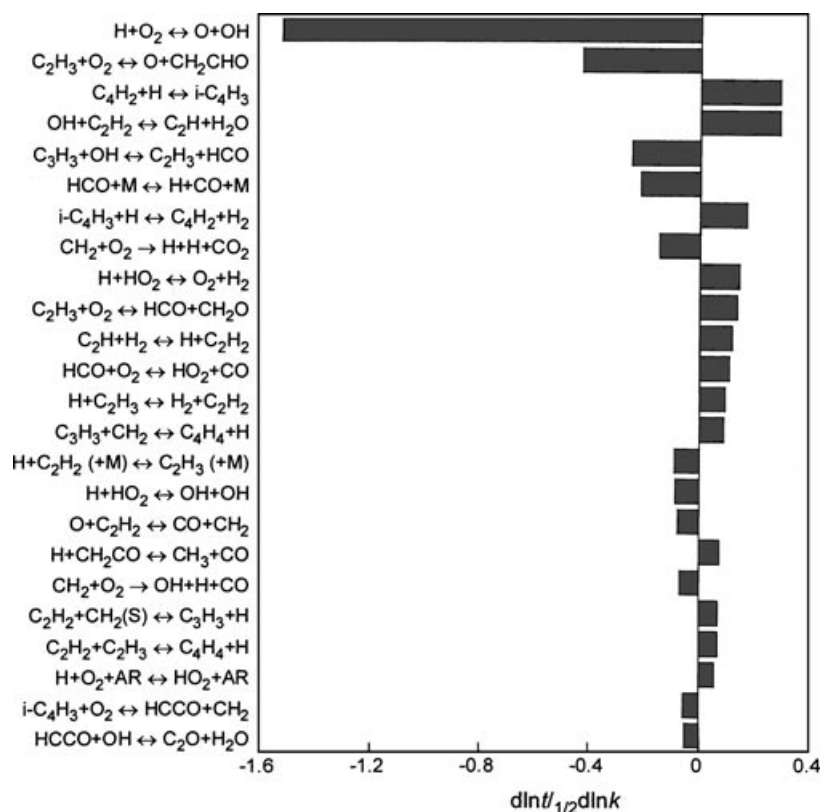


Figure 8 Logarithmic response sensitivities of the half-decay time $t_{1/2}$ of O_2 concentration computed for the experimental conditions of Fig. 7 with Model 0. Only values above 0.05 are shown.

differences between the predictions of Models 0 and 1 for the conditions of Fig. 7).

Comparison of the sensitivity spectra shown in Figs. 5 and 8 indicates that the optimization variables common to our experimental data and those of Hidaka et al. [24] are k_{22} , k_{24a} , and k_{24b} . As was shown in the previous section, the sensitivity of our targets to k_{24a} , and k_{24b} is only marginal. This leaves k_{22} as the only optimization variable common to the both data sets. Having examined the behavior of k_{22} under the conditions of our experiments (Cases XXVIII–XXXIX in Table IV), we now focus on the analysis of the Hidaka et al.'s data.

In addition to the chosen rate coefficients, we included the enthalpies of formation $\Delta_f H_{298}^\circ$ of C_3H_2 , $i-C_4H_3$, and $n-C_4H_3$ as optimization variable because of the large uncertainties in the thermodynamic data of these species. A screening sensitivity analysis showed that with a decrease in the enthalpy of formation of C_3H_2 the influence of reaction



increases. Reaction (27) was proposed by Miller and

Melius [41] and included into their kinetic mechanism with a rate coefficient of $5.0 \times 10^{13} \text{ cm}^3 \text{ mol}^{-1} \text{ s}^{-1}$. It was modified in a later study [79] to a significantly lower value, $2.0 \times 10^{12} e^{-503/T} \text{ cm}^3 \text{ mol}^{-1} \text{ s}^{-1}$. In light of these facts, we added k_{27} to the optimization variables.

Optimization Results

The results of several optimization runs are summarized in Table VI. Case *HI* corresponds to the base mechanism, Model 0. Case *HII* is an unconstrained optimization run. It resulted in a simultaneous twofold decrease in rate coefficients k_{24a} and k_{24b} and hence in the total rate coefficient of reaction (24). Model 0 employs k_{24} taken from the multichannel RRKM calculations of Mebel et al. [120] which are in excellent agreement with consensus experimental values at temperatures below 1000 K (see, e.g., Knyazev and Slagle [121]). On this basis, a twofold reduction in k_{24} is unacceptable. Fixing k_{24a} and k_{24b} at the Model 0 expressions (Case *HIII*) produced approximately the same quality of fit to experimental data as Case *HII*. Therefore, the rate coefficients of reactions (24a)

Table VI Results of Model Optimization Against Hidaka et al.'s Targets in Table V

Case	Optimization Variables ^a									Objective Function Φ
	Reaction Rate Coefficients						Species Enthalpies, Δh			
	A_{22}	A_{24a}	A_{24b}	A_{25}	A_{26}	A_{27}	C_3H_2	$i-C_4H_3$	$n-C_4H_3$	
<i>HI</i>	1	1	1	1	1	<u>4.00</u>	0	0	0	3.53
<i>HII</i>	3.00 ⁺	0.50 ₋	0.58	2.19	3.00 ⁺	0.13 ₋	5.00 ₋	3.16	5.00 ₋	0.080
<i>HIII</i>	1.81	1	1	2.41	0.33 ₋	0.13 ₋	5.00 ₋	0.76	2.50 ₋	0.090
<i>HIV</i>	1.84	1	1	2.59	0.33 ₋	0.13 ₋	4.00 ₋	0.83	2.50 ₋	0.093
<i>HV</i>	1.84	1	1	2.73	0.33 ₋	0.13 ₋	3.00 ₋	0.94	2.50 ₋	0.096
<i>HVI</i>	1.94	1	1	2.60	0.33 ₋	0.25 ₋	5.00 ₋	0.72	2.50 ₋	0.091
<i>HVII</i>	2.24	1	1	3.00 ⁺	0.33 ₋	0.18 ₋	0	0	0	0.110
<i>HVIII</i>	2.36	1	1	3.00 ⁺	0.33 ₋	0.25 ₋	0	0	0	0.111
<i>HIX</i>	2.02	1	1	2.93	0.33 ₋	0.25 ₋	4.00 ₋	0	0	0.099
<i>HX</i>	2.05	1	1	2.93	0.33 ₋	0.25 ₋	0	1.14	4.00 ₋	0.100
<i>HXI</i>	1.96	1	1	2.78	0.33 ₋	0.25 ₋	4.00 ₋	0.77	2.00 ₋	0.095
<i>HXII</i>	1.50 ⁺	1	1	3.00 ⁺	0.33 ₋	0.25 ₋	3.00 ₋	2.34	2.40 ₋	0.115
<i>HXIII</i>	1.50 ⁺	1	1	2.50 ⁺	0.33 ₋	0.25 ₋	4.00 ₋	2.95	3.00 ₋	0.133
<i>HXIV</i>	1.50 ⁺	1	1	2.50 ⁺	0.33 ₋	0.25 ₋	3.00 ₋	3.33	2.50 ₋	0.148
<i>HXV</i>	1.50 ⁺	1	1	3.00 ⁺	0.50 ₋	0.25 ₋	3.00 ₋	3.36	2.50 ₋	0.153
<i>HXVI</i>	2.66	1	1	3.00 ⁺	0.33 ₋	0.50 ₋	0	0	0	0.116
<i>HXVII</i>	3.00 ⁺	1	1	3.00 ⁺	0.33 ₋	1.00 ₋	0	0	0	0.132
<i>HXVIII</i>	3.00 ⁺	1	1	3.00 ⁺	<u>1.00</u>	0.25 ₋	0	0	0	0.223
<i>HXIX</i>	3.00 ⁺	1	1	<u>1.00</u>	0.33 ₋	0.25 ₋	0	0	0	0.996
<i>HXX</i>	1.50 ⁺	1	1	3.00 ⁺	0.33 ₋	0.25 ₋	0	0	0	0.325
<i>HXXI</i>	1.50 ⁺	1	1	3.00 ⁺	0.33 ₋	0.25 ₋	4.00 ₋	1.97	2.00 ₋	0.108

^a Entry designations are as follows. For A_{22} through A_{26} , 1 indicates that the corresponding rate coefficient was fixed at the Model 0 expression. For A_{27} the numbers listed are multiplication factors to the Pauwels et al.'s expression [79]. For species enthalpies, 0 indicates that the corresponding standard enthalpy of formation was fixed at the G3 result, $\Delta_f^{G3} H_{298}^\circ = 127.4, 116,$ and 126.2 kcal mol⁻¹ for $C_3H_2, i-C_4H_3,$ and $n-C_4H_3,$ respectively, and for the nonzero entries $\Delta_f H_{298}^\circ = \Delta_f^{G3} H_{298}^\circ - \Delta h$ (kcal mol⁻¹). Numerical entry followed by the + (in superscript) or - (in subscript) sign indicates that the optimization variable reached the upper or lower boundary of the optimization range, respectively. Underlined numerical entry indicates that the value was fixed during the optimization.

and (24b) were not included into further optimization runs.

The rest of the runs in Table VI report the results of various constrained optimizations, looking for a suitable compromise between the kinetic and thermodynamic changes required to reconcile the model and Hidaka et al.'s targets. Cases *HIV*–*HXI* show that the optimized values of k_{22} were about twice higher than the initial, Model 0 value. Comparing these optimization runs to Cases *XXVIII*–*XXXIX* in Table IV, those testing k_{22} on our targets, shows opposite trends. As a compromise, we chose a multiplier of 1.50 for A_{22} .

After an additional series of optimization runs, testing further constraints (Cases *HXII*–*HXXI*), we selected the Case *HXXI* as the *best current* compromise for the Hidaka et al.'s targets. It combines acceptable (see below) kinetic and thermodynamic changes with a relatively low value of $\Phi_{HXXI} = 0.108$, not far removed from the unconstrained minimum of $\Phi_{HII} = 0.080$.

CONCLUSIONS

On the basis of the present analysis of our and Hidaka et al.'s experimental data along with the assessment of uncertainties in the pertinent thermochemical data, our choice for the *best current* parameter set is a combination of the results from Case *XXXVIII* in Table IV and Case *HXXI* in Table VI. This parameter set is summarized in Table VII and the corresponding reaction model is designated as Model 2. Many aspects of the parameter changes were addressed in the previous sections, while discussing the results of and motivation for the performed optimization runs. The most noteworthy of these changes are as follows:

- Model 2 makes a compromise to the branching ratio of reaction (21), increasing it from 0.33 in Model 1 to 0.4, closer to an average literature value of 0.66 used in GRI-Mech 3.0.

Table VII Best Current Parameter Set

	Model Parameter	Parameter Values ^a	Source/Action
k_6	$C_2H_2 + M \rightarrow H_2CC: + M$	$2.45 \times 10^{15} T^{-0.64} e^{-25010/T}$	[25]
k_{7b}	$H_2CC: + O_2 \rightarrow CH_2 + CO_2$	3.3×10^{12}	$k_{[25]}/3$
k_{8a}	$HCCO + O_2 \rightarrow OH + 2CO$	$4.2 \times 10^{10} e^{-430/T}$	[46]
k_9	$C_2H + H_2 \rightarrow H + C_2H_2$	$4.45 \times 10^6 T^{2.22} e^{-461/T}$	fit, Fig. 3
k_{10}	$C_2H + C_2H_2 \rightarrow H + C_4H_2$	$1.94 \times 10^{13} T^{0.238} e^{37/T}$	fit, Fig. 4
k_{21a}	$O + C_2H_2 \rightarrow CO + CH_2$	$1.25 \times 10^7 T^{2.0} e^{-956/T}$	$k_{GRI-Mech\ 3.0} \times 1.8$
k_{21b}	$O + C_2H_2 \rightarrow H + HCCO$	$8.1 \times 10^6 T^{2.0} e^{-956/T}$	$k_{GRI-Mech\ 3.0} \times 0.60$
k_{22}	$OH + C_2H_2 \rightarrow C_2H + H_2O$	$5.06 \times 10^7 T^{2.0} e^{-7046/T}$	$k_{[122]} \times 1.5$
k_{23}	$CH_2 + O_2 \rightarrow 2H + CO_2$	$5.8 \times 10^{12} e^{-755/T}$	GRI-Mech 3.0
k_{24a}	$C_2H_3 + O_2 \rightarrow O + CH_2CHO$	$3.03 \times 10^{11} T^{0.3} e^{5.5/T}$	[120]
k_{24b}	$C_2H_3 + O_2 \rightarrow HCO + CH_2O$	$4.58 \times 10^{16} T^{-1.4} e^{-511/T}$	[120]
k_{25}	$C_4H_2 + H \rightarrow i-C_4H_3$	$3.3 \times 10^{30} T^{-4.92} e^{-5435/T}$	$k_{[47]} \times 3$
k_{26}	$C_3H_3 + OH \rightarrow C_2H_3 + HCO$	1.33×10^{13}	$k_{[47]}/3$
k_{27}	$C_3H_2 + O_2 \rightarrow HCCO + H + CO$	$1.25 \times 10^{11} e^{-503/T}$	$k_{[79]} \times 0.0625$
	$\Delta_f H_{298}^\circ(C_3H_2)$	123.4	See text
	$\Delta_f H_{298}^\circ(i-C_4H_3)$	114.0	See text
	$\Delta_f H_{298}^\circ(n-C_4H_3)$	124.2	See text

^a Units are $\text{cm}^3 \text{mol}^{-1} \text{s}^{-1}$ for rate coefficients and kcal mol^{-1} for enthalpies of formation.

- The pre-exponential factor of k_{22} is increased by 50% from Miller and Melius' recommendation [122]. All optimization cases for the Hidaka et al.'s targets show a persistent upward trend for this rate coefficient, either reaching the upper boundary when constrained or doubling its value when left free (Table VI). On the other hand, Cases XXVIII–XXXIX in Table IV show that increasing k_{22} deteriorates the quality of fit for our own targets: raising it by factors of 1.5 and 2 increases the objective function by 25 and 50%, respectively, from Case XIX. Our choice of a 50% increase in k_{22} is a compromise between the two trends; we consider it to be feasible in light of the scatter in reported experimental data on this reaction (see, e.g., Baulch et al. [101]).
- Rate coefficient k_{26} of Model 0 is an estimated value [47] and hence a factor of 3 decrease in k_{26} is not prohibitive.
- The decrease of k_{27} by a factor of 16 from Ref. [79] is the largest change suggested by Model 2. It follows a definite trend seen in our optimization runs (Table IV). The reduction can be rationalized considering the 1,3-diradical structure of C_3H_2 and is consistent with the increased stability of C_3H_2 radical. Also, k_{27} in Model 2 is closer in magnitude to the experimental result of $3.0 \times 10^{10} e^{-1443/T} \text{ cm}^3 \text{mol}^{-1} \text{s}^{-1}$ reported [37] for reaction $C_3H_3 + O_2 \rightarrow HCO + CH_2CO$.
- The Model 2 value for the enthalpy of formation of C_3H_2 , $\Delta_f H_{298}^\circ(C_3H_2) = 123.4 \text{ kcal mol}^{-1}$, is in

the midst of estimates [17] based on recent experimental values for $c\text{-}C_3H_2$ [74,77] and quantum ab initio calculations of the difference between C_3H_2 and $c\text{-}C_3H_2$ [41,75,82,85–89].

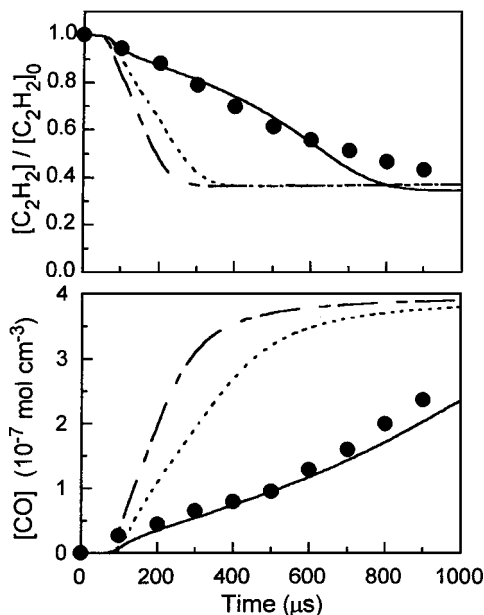


Figure 9 Observed and calculated species profiles. Top panel: Relative C_2H_2 concentration in a 4.0% C_2H_2 –2.0% O_2 –Ar mixture at $T_0 = 1343 \text{ K}$ and $C_0 = 13.4 \text{ mol m}^{-3}$. Bottom panel: CO concentration in a 4.0% C_2H_2 –2.0% O_2 –Ar mixture at $T_0 = 1292 \text{ K}$ and $C_0 = 13.0 \text{ mol m}^{-3}$. ●, experiment (Hidaka et al. [24]); ----, Model LW; ·····, Model 2; —, Model 0.

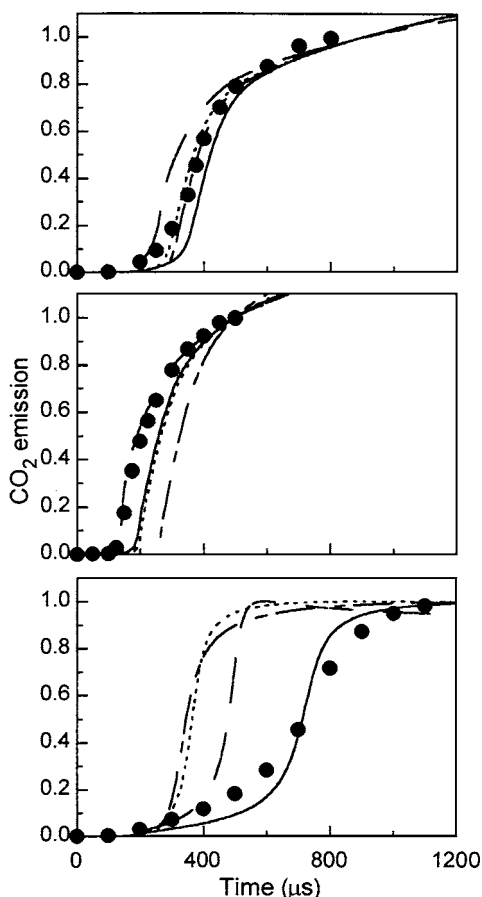


Figure 10 Observed and calculated CO emission profiles at $4.24 \mu\text{m}$. Top panel: 1.0% C_2H_2 -2.5% O_2 -Ar, $T_0 = 1221 \text{ K}$, $C_0 = 14.5 \text{ mol m}^{-3}$. Middle panel: 1.0% C_2H_2 -5.0% O_2 -Ar, $T_0 = 1214 \text{ K}$, $C_0 = 14.5 \text{ mol m}^{-3}$. Bottom panel: 2.0% C_2H_2 -2.5% O_2 -Ar, $T_0 = 1179 \text{ K}$, $C_0 = 14.3 \text{ mol m}^{-3}$. ●, experiment (Hidaka et al. [24]); ---, Model H; - - -, Model LW; ·····, Model 0; —, Model 2.

- The optimization results for the enthalpies of formation of $i\text{-C}_4\text{H}_3$ and $n\text{-C}_4\text{H}_3$ radicals, obtained in fitting the reaction model against the Hidaka et al.'s targets, exhibit a definite downward trend. The Model 2 choices are within the current range of reported estimates [16,20,21,24,25,41,47,56,95–98], with a difference of about 10 kcal mol^{-1} between the two isomers, the middle grounds among recent theoretical predictions [98].

Model 2 fits our experimental targets almost as good as Model 1 (see bottom panel of Fig. 2), with relative errors of $+25/-20\%$, over the entire temperature range studied. At the same time, contrary to Model 1, Model 2 also reproduces closely the experimental data of Hidaka et al. [24], as demonstrated in Figs. 7, 9,

and 10. This is not to say that Model 2 is the best possible model. On the contrary, we use language “best current” to qualify the result of the present modeling effort, emphasizing the transient nature of the process of derivation of reaction models we advocate in general [23,99] and practice in the present study. The ability to reconcile the two sets of experimental data, ours and Hidaka et al.'s, did not come “easy” but required some difficult and possibly problematic choices. Model 2 represents our *best* assessment of the *current* data and their associate uncertainties. It is a noteworthy feature of the employed numerical procedure that possible tradeoffs are expressed in rigorous quantitative terms. One can create a different *best current model* by changing optimization constraints, either as a result of personal preferences or by adding new data as they become available (for instance, an anonymous Reviewer suggested decreasing k_{24a} based on very recent reports [123,124]). The present recommendation, summarized in Table VII, is offered in expectation that the development of acetylene combustion mechanism will continue, with inclusion of larger data sets and broader participation of the community in the process.

BIBLIOGRAPHY

1. Glassman, I. Combustion; Academic Press: Orlando, FL, 1996.
2. Turns, S. R. An Introduction to Combustion: Concepts and Applications; McGraw-Hill: New York, 2000.
3. Spear, K. E.; Dismukes, J. P. (Eds.) Synthetic Diamond: Emerging CVD Science and Technology; Wiley: New York, 1994.
4. Frenklach, M.; Ebert, L. B. J Phys Chem 1988, 92, 561.
5. Richter, H.; Grieco, W. J.; Howard, J. B. Combust Flame 1999, 119, 1.
6. Frenklach, M.; Feigelson, E. In From Stardust to Planetsimals; Pendleton, Y. J.; Tielens, A. G. G. M. (Eds.); Astronomical Society of the Pacific: San Francisco, 1997; p. 107.
7. Palmer, H. B.; Cullis, C. F. In Chemistry and Physics of Carbon; Walker, P. L. (Ed.); Marcel Dekker: New York, 1965; p. 265.
8. Haynes, B. S.; Wagner, H. G. Prog Energy Combust Sci 1981, 7, 229.
9. Frenklach, M. Phys Chem Chem Phys 2002, 4, 2028.
10. Varatharajan, B.; Williams, F. A. Combust Flame 2001, 125, 624.
11. Charlston-Goch, D.; Chadwick, B. L.; Morrison, R. J. S.; Campisi, A.; Thomsen, D. D.; Laurendeau, N. M. Combust Flame 2001, 125, 729.
12. Yuan, T.; Wang, C.; Yu, C.-L.; Frenklach, M.; Rabinowitz, M. J Phys Chem 1991, 95, 1258.
13. Yu, C.-L.; Wang, C.; Frenklach, M. J Phys Chem 1995, 99, 14377.

14. Eiteneer, B.; Yu, C.-L.; Goldenberg, M.; Frenklach, M. *J Phys Chem* 1998, 102, 5196.
15. Colket, M. B.; Seery, D. J.; Palmer, H. B. *Combust Flame* 1989, 75, 343.
16. Colket, M. B.; Seery, D. J.; Palmer, H. B. *Combust Flame* 1991, 84, 434.
17. Eiteneer, B. N. PhD Thesis, University of California at Berkeley, 2000.
18. Gardiner, W. C., Jr.; Walker, B. F.; Wakefield, C. B. In *Shock Waves in Chemistry*; Lifshitz, A. (Ed.); Dekker: New York, 1981; p. 319.
19. McBride, B. J.; Gordon, S.; Reno, M. A. NASA TM-4513, 1993.
20. Burcat, A.; McBride, B. J. *Technion TAE* 697, 1993.
21. Burcat, A. <http://garfield.chem.elte.hu/Burcat/burcat.html>.
22. Eiteneer, B.; Frenklach, M. *J Phys Chem* 2000, 104, 9797.
23. Smith, G. P.; Golden, D. M.; Frenklach, M.; Moriarty, N. W.; Eiteneer, B.; Goldenberg, M.; Bowman, C. T.; Hanson, R.; Song, S.; Gardiner, W. C.; Lissianski, V.; Qin, Z. http://http://www.me.berkeley.edu/gri_mech/.
24. Hidaka, Y.; Hattori, K.; Okuno, T.; Inami, K.; Abe, T. *Combust Flame* 1996, 107, 401.
25. Laskin, A.; Wang, H. *Chem Phys Lett* 1999, 303, 43.
26. Colket, M. B.; Naegeli, D. W.; Glassman, I. *Int J Chem Kinet* 1975, 7, 223.
27. Tanzawa, T.; Gardiner, W. C., Jr. *Combust Flame* 1980, 39, 241.
28. Miller, J. A.; Mitchell, R. E.; Smooke, M. D.; Kee, R. J. *Proc Combust Inst* 1982, 19, 181.
29. Warnatz, J.; Bockhorn, H.; Moser, A.; Wenz, H. *Proc Combust Inst* 1983, 19, 841.
30. Warnatz, J. In *Combustion Chemistry*; Gardiner, W. C., Jr. (Ed.); Springer-Verlag: New York, 1984; p. 197.
31. Perry, R. A. *Combust Flame* 1984, 58, 221.
32. Scherzer, K.; Claus, P.; Karwath, M. *Z Phys Chem* 1985, 266, 321.
33. Tsang, W.; Hampson, R. F. *J Phys Chem Ref Data* 1986, 15, 1087.
34. Frank, P.; Bhaskaran, K. A.; Just, T. *Proc Combust Inst* 1986, 21, 885.
35. Wu, C. H.; Singh, H. J.; Kern, R. D. *Int J Chem Kinet* 1987, 19, 975.
36. Dean, A. M.; Westmoreland, P. R. *Int J Chem Kinet* 1987, 19, 207.
37. Slagle, I. R.; Gutman, D. *Proc Combust Inst* 1988, 22, 875.
38. Miller, J. A.; Bowman, C. T. *Prog Energy Combust Sci* 1989, 15, 287.
39. Kern, R. D.; Xie, K.; Chen, H.; Kiefer, J. H. *Proc Combust Inst* 1990, 23, 69.
40. Tsang, W. *J Phys Chem Ref Data* 1991, 20, 221.
41. Miller, J. A.; Melius, C. F. *Combust Flame* 1992, 91, 21.
42. Wang, H. Ph. D. Thesis, Pennsylvania State University, 1992.
43. Bozzelli, J. W.; Dean, A. M. *J Phys Chem* 1993, 97, 4427.
44. Baulch, D. L.; Cobos, C. J.; Cox, R. A.; Frank, P.; Hayman, G.; Just, T.; Kerr, J. A.; Murrells, T.; Pilling, M. J.; Troe, J.; Walker, R. W.; Warnatz, J. *J Phys Chem Ref Data* 1994, 23, 847.
45. Frenklach, M.; Wang, H. In *Soot Formation in Combustion: Mechanisms and Models*; Bockhorn, H. (Ed.); Springer-Verlag: Berlin, 1994; p. 165.
46. Hidaka, Y.; Kimura, K.; Hattori, K.; Okuno, T. *Combust Flame* 1996, 106, 155.
47. Wang, H.; Frenklach, M. *Combust Flame* 1997, 110, 173.
48. Wodtke, A. M.; Lee, Y. T. *J Phys Chem* 1985, 89, 4744.
49. Green, P. G.; Kinsey, J. L.; Field, R. W. *J Chem Phys* 1989, 91, 5160.
50. Segall, J.; Lavi, R.; Wen, Y.; Wittig, C. *J Phys Chem* 1989, 93, 7287.
51. Ervin, K. M.; Gronert, S.; Barlow, S. E.; Gilles, M. K.; Harrison, A. G.; Bierbaum, V. M.; DePuy, C. H.; Lineberger, W. C.; Ellison, G. B. *J Am Chem Soc* 1990, 112, 5750.
52. Habibollahzadeh, D.; Murray, J. S.; Grodzicki, M.; Seminario, J. M.; Politzer, P. *Int J Quantum Chem* 1992, 42, 267.
53. Mordaunt, D. H.; Ashfold, M. N. R. *J Chem Phys* 1994, 101, 2630.
54. Partridge, H.; Bauschlicher, C. W., Jr. *J Chem Phys* 1995, 103, 10589.
55. Peterson, K. A.; Dunning, T. H., Jr. *J Chem Phys* 1997, 106, 4119.
56. Kiefer, J. H.; Von Drasek, W. A. *Int J Chem Kinet* 1990, 22, 747.
57. Gardiner, W. C.; Walker, B. F. *J Chem Phys* 1968, 48, 5279.
58. Jachimowski, C. *J Combust Flame* 1977, 29, 55.
59. Duran, R. P.; Amorebieta, V. T.; Colussi, A. J. *J Phys Chem* 1988, 92, 636.
60. Kiefer, J. H.; Sidhu, S. S.; Kern, R. D.; Xie, K.; Chen, H.; Harding, L. B. *Combust Sci Technol* 1992, 82, 101.
61. Gallo, M. M.; Hamilton, T. P.; Schaefer, H. F., III. *J Am Chem Soc* 1990, 112, 8714.
62. Jones, I. T. N.; Bayes, K. D. *Proc R Soc London Ser A* 1973, 335, 547.
63. Peeters, J.; Schaekers, M.; Vinckier, C. *J Phys Chem* 1986, 90, 6552.
64. Farhat, S. K.; Morter, C. L.; Glass, G. P. *J Phys Chem* 1993, 12789.
65. Stephens, J. W.; Hall, J. L.; Solka, H.; Yan, W.-B.; Curl, R. F.; Glass, G. P. *J Phys Chem* 1987, 91, 5740.
66. Lander, D. R.; Unfried, K. G.; Glass, G. P.; Curl, R. F. *J Phys Chem* 1990, 94, 7759.
67. Koshi, M.; Nishida, N.; Matsui, H. *J Phys Chem* 1992, 96, 5875.
68. Koshi, M.; Fukuda, K.; Kamiya, K.; Matsui, H. *J Phys Chem* 1992, 96, 9839.
69. Opansky, B. J.; Leone, S. R. *J Phys Chem* 1996, 100, 19904.

70. Peeters, J.; Van Look, H.; Ceursters, B. *J Phys Chem* 1996, 100, 15124.
71. Kruse, T.; Roth, P. *J Phys Chem A* 1997, 101, 2138.
72. Shin, K. S.; Michael, J. V. *J Phys Chem* 1991, 95, 5864.
73. Pedersen, J. O. P.; Opansky, B. J.; Leone, S. R. *J Phys Chem* 1993, 97, 6822.
74. Clauberg, H.; Minsek, D. W.; Chen, P. *J Am Chem Soc* 1992, 114, 99.
75. Jonas, V.; Bohme, M.; Frenking, G. *J Phys Chem* 1992, 96, 1640.
76. Herges, R.; Mebel, A. *J Am Chem Soc* 1994, 116, 8229.
77. Chyall, L. J.; Squires, A. A. *Int J Mass Spectrom Ion Proc* 1995, 150, 257.
78. Kern, R. D.; Chen, H.; Kiefer, J. H.; Mudipalli, P. S. *Combust Flame* 1995, 100, 177.
79. Pauwels, J.-F.; Volponi, J. V.; Miller, J. A. *Combust Sci Technol* 1995, 110/111, 249.
80. Robinson, M. S.; Polak, M. L.; Bierbaum, V. M.; DePuy, C. H.; Lineberger, W. C. *J Am Chem Soc* 1995, 117, 6766.
81. Miller, J. A.; Volponi, J. V.; Pauwels, J.-F. *Combust Flame* 1996, 105, 451.
82. Takahashi, J.; Yamashita, K. *J Chem Phys* 1996, 104, 6613.
83. Jackson, W. M.; Mebel, A. M.; Lin, S. H.; Lee, Y. T. *J Phys Chem A* 1997, 101, 6638.
84. Kiefer, J. H.; Mudipalli, P. S.; Sidhu, S. S.; Kern, R. D.; Jursic, B. S.; Xie, K.; Chen, H. *J Phys Chem A* 1997, 101, 4057.
85. Ochsenfeld, C.; Kaiser, R. I.; Lee, Y. T.; Suits, A. G. *J Chem Phys* 1997, 106, 4141.
86. Seburg, R. A.; Patterson, E. V.; Stanton, J. F.; McMahon, R. J. *J Am Chem Soc* 1997, 119, 5847.
87. Guadagnini, R.; Schatz, G. C.; Walch, S. P. *J Phys Chem A* 1998, 102, 5857.
88. Mebel, A. M.; Jackson, W. M.; Chang, A. H. H.; Lin, S. H. *J Am Chem Soc* 1998, 120, 5751.
89. Vereecken, L.; Pierloot, K.; Peeters, J. *J Chem Phys* 1998, 108, 1068.
90. Vereecken, L.; Peeters, J. *J Phys Chem A* 1999, 103, 5523.
91. Seburg, R. A.; DePinto, J. T.; Patterson, E. V.; McMahon, R. J. *J Am Chem Soc* 1995, 117, 835.
92. Boullart, W.; Devriendt, K.; Borms, R.; Peeters, J. *J Phys Chem* 1996, 100, 998.
93. Deyler, H.-J.; Fischer, I.; Chen, P. *J Chem Phys* 1999, 111, 3441.
94. Moriarty, N. W.; Eiteneer, B. Personal communication, 1990.
95. Melius, C. F. <http://www.ca.sandia.gov/HiTemp-Thermo/>.
96. Kee, R. J.; Rupley, F. M.; Miller, J. A. SAND89-8009B UC-706, Sandia Laboratories, 1993.
97. Cioslowski, J.; Liu, G.; Moncrieff, D. *J Phys Chem A* 1999, 103, 11465.
98. Krokidis, X.; Moriarty, N. W.; Lester, W. A., Jr.; Frenklach, M. *Int J Chem Kinet* 2001, 33, 808.
99. Frenklach, M.; Wang, H.; Rabinowitz, M. *J. Prog Energy Combust Sci* 1992, 18, 47.
100. Yu, C.-L.; Frenklach, M.; Masten, D. A.; Hanson, R. K.; Bowman, C. T. *J Phys Chem* 1994, 98, 4770.
101. Baulch, D. L.; Cobos, C. J.; Cox, R. A.; Esser, C.; Frank, P.; Just, T.; Kerr, J. A.; Pilling, M. J.; Troe, J.; Walker, R. W.; Warnatz, J. *J Phys Chem Ref Data* 1992, 21, 411.
102. Sullivan, J. O.; Warneck, P. *J Phys Chem* 1965, 69, 1749.
103. Niki, H. *J Chem Phys* 1967, 47, 3102.
104. Brown, J. M.; Thrush, B. A. *Trans Faraday Soc* 1967, 63, 630.
105. James, G. S.; Glass, G. P. *J Chem Phys* 1969, 50, 2268.
106. Hoyermann, K.; Wagner, H. G.; Wolfrum, J. *Z Phys Chem* 1969, 63, 193.
107. Westenberg, A. A.; deHaas, N. *J Phys Chem* 1969, 73, 1181.
108. Stuhl, F.; Niki, H. *J Chem Phys* 1971, 55, 3954.
109. Peeters, J.; Mahnen, G. *Proc Combust Inst* 1973, 14, 133.
110. Vandooren, J.; Van Tiggelen, P. *J. Proc Combust Inst* 1977, 16, 1133.
111. Westenberg, A. A.; deHaas, N. *J Chem Phys* 1977, 66, 4900.
112. Aleksandrov, E. N.; Arutyunov, V. S.; Kozlov, S. N. *Kinet Katal* 1981, 22, 391.
113. Lohr, R.; Roth, P. *Ber Bunsen-Ges Phys Chem* 1981, 85, 153.
114. Homann, K. H.; Wellmann, C. *Ber Bunsen-Ges Phys Chem* 1983, 87, 527.
115. Mahmud, K.; Fontijn, A. *J Phys Chem* 1987, 91, 1918.
116. Russell, J. J.; Senkan, S. M.; Seetula, J. A.; Gutman, D. *Proc Combust Inst* 1988, 22, 1007.
117. Bohn, B.; Stuhl, F. *J Phys Chem* 1990, 94, 8010.
118. Michael, J. V.; Wagner, A. F. *J Phys Chem* 1990, 94, 2453.
119. Harding, L. B.; Wagner, A. F. *J Phys Chem* 1986, 90, 2974.
120. Mebel, A. M.; Diau, E. W. G.; Lin, M. C.; Morokuma, K. *J Am Chem Soc* 1996, 118, 9759.
121. Knyazev, V. D.; Slagle, I. R. *J Phys Chem* 1995, 99, 2247.
122. Miller, J. A.; Melius, C. F. *Proc Combust Inst* 1988, 22, 1031.
123. Qin, Z.; Lissianski, V. V.; Yang, H.; Gardiner, W. C.; Davis, S.; Wang, H. *Proc Combust Inst* 2000, 28, 1663.
124. Carriere, T.; Westmoreland, P. R. *Proc Combust Inst*; (in press).